Time-resolved-correlation measurements of temporally heterogeneous dynamics

Agnès Duri,[1] Hugo Bissig,[2] Véronique Trappe,[2] and Luca Cipelletti[1,*]
[1]*Laboratoire des Colloïdes, Verres et Nanomatèriaux (UMR 5587), Université Montpellier 2 and CNRS, 34095 Montpellier Cedex 5, France*
[2]*Department de Physique, Université de Fribourg, Chemin du Musée 3, 1700 Fribourg, Suisse*
(Received 1 August 2005; published 28 November 2005)

Time resolved correlation (TRC) is a recently introduced light scattering technique that allows one to detect and quantify dynamic heterogeneities. The technique is based on the analysis of the temporal evolution of the speckle pattern generated by the light scattered by a sample, which is quantified by $c_I(t,\tau)$, the degree of correlation between speckle images recorded at time t and $t+\tau$. Heterogeneous dynamics results in significant fluctuations of $c_I(t,\tau)$ with time t. We describe how to optimize TRC measurements and how to detect and avoid possible artifacts. The statistical properties of the fluctuations of c_I are analyzed by studying their variance, probability distribution function, and time autocorrelation function. We show that these quantities are affected by a noise contribution due to the finite number N of detected speckles. We propose and demonstrate a method to correct for the noise contribution, based on a $N\rightarrow\infty$ extrapolation scheme. Examples from both homogeneous and heterogeneous dynamics are provided. Connections with recent numerical and analytical works on heterogeneous glassy dynamics are briefly discussed.

DOI: 10.1103/PhysRevE.72.051401 PACS number(s): 82.70.−y, 42.30.Ms, 64.70.Pf, 05.40.−a

I. INTRODUCTION

Soft glassy systems such as concentrated colloidal suspensions, emulsions, surfactant phases, gels, and foams exhibit very slow and unusual dynamics, characterized by nonexponential relaxations of correlation and response functions, which often depend on sample history and may be heterogeneous both in space and time [1]. These phenomena have attracted a great interest, in part due to their "universal" character. Examples of unifying descriptions are the mode coupling theory of the stationary average dynamics of concentrated suspensions of particles with both repulsive or attractive interactions [2–4] or, at a more qualitative level, the concept of jamming, which rationalizes the fluid-to-solid transition in a wide range of systems and experimental configurations [5]. Additionally, soft glassy materials often exhibit intriguing similarities with hard condensed matter glasses, such as the dependence of the dynamics on sample history (aging phenomena [6,7], rejuvenation and memory effects [8,9]) or the presence of dynamical heterogeneity [10–12].

Light scattering is a popular means to measure the average dynamics. In a traditional dynamic light scattering experiment, one measures the normalized time autocorrelation function of the scattered intensity $g_2(\tau)=\overline{I_1(t)I_1(t+\tau)}/\overline{I_1(t)}^2$, where the average $\overline{\cdots}$ is over time t and $I_1(t)$ is the intensity collected by a single detector. The intensity autocorrelation function provides quantitative information on the dynamics of the sample; the way this information is extracted depends on the experimental configuration. In single scattering experiments, $g_2(\tau)$ is related to the intermediate scattering function $f(\tau)$ via the Siegert relation $f(\tau)=\sqrt{\beta^{-1}[g_2(\tau)-1]}$, where β is the coherence factor that depends on the size ratio between the speckle—or coherence area—and the detector [13,14]. In the opposite limit of strong multiple scattering, the diffusing-wave spectroscopy (DWS) formalism [15] allows the particle mean square displacement to be calculated from $g_2(\tau)-1$, provided that the dynamics be spatially and temporally homogeneous. For glassy systems the average over time required to compute $g_2(\tau)$ may become in practice unfeasible, either because the dynamics is so slow that prohibitively long experiments would be required to accumulate a satisfactory statistics, or because the dynamics may be nonstationary, e.g., for aging systems. Various schemes have been introduced to address this issue, most of them based on the idea of measuring $g_2(\tau)$ for many independent speckles and averaging the intensity correlation function not only over time, but also over distinct speckles. This can be done either sequentially—e.g., by slowly rotating the sample so as to illuminate a single detector with different speckles (interleave [16] or echo [17] methods [18])—or in parallel, e.g., by using the pixels of a charge-coupled device camera (CCD) as independent detectors (multispeckle method [19–21]).

These techniques drastically reduce the required time average and thus extend the applicability of light scattering to glassy systems. Similarly to traditional light scattering measurements, however, they provide information only on the average dynamics, not on its fluctuations. However, recent theoretical and simulation works suggest that dynamic heterogeneity is a key feature of the slow dynamics in glassy systems. In view of the very limited number of experiments that directly test this behavior on soft glasses [10,11], new experimental tools that access fluctuations of the dynamics are needed. We have recently introduced the time resolved correlation (TRC) scheme [22], a method that allows temporally heterogeneous dynamics to be investigated by scattering techniques. The idea at the heart of TRC is that the temporal evolution of the speckle pattern generated by the

*Electronic address: lucacip@lcvn.univ-montp2.fr

scattered light will be very different for homogeneous *vs*. heterogeneous dynamics. For homogeneous dynamics, we expect the speckle images to change smoothly in time. By contrast, for heterogeneous dynamics the speckle pattern is expected to evolve discontinuously, because the rate of change of the sample configuration will not be constant but rather fluctuate with time. Experimentally, the speckle images are recorded by a CCD camera and their evolution is quantified by introducing $c_I(t,\tau)$, the degree of correlation between images taken at time t and $t+\tau$ (a rigorous definition will be given in Sec. II). Inspection of the t dependence of c_I at fixed τ allows temporally heterogeneous dynamics to be discriminated from homogeneous dynamics. Indeed, in the former case a large drop (increase) of c_I is observed whenever the dynamics is faster (slower) than average, while in the latter the degree of correlation is constant. This method is quite general, since it can be applied to any experimental configuration where a multielement detector can be used to record the speckle pattern generated by a sample illuminated by coherent radiation. Examples are CCD-based light scattering experiments in the single scattering regime, both at wide [20] and small angle [21], DWS in the transmission [23] or backscattering [24] geometry, and x-photon correlation spectroscopy (XPCS) at small angles [25]. In principle, the technique could also be extended to nonelectromagnetic radiation, e.g., to acoustic DWS [26].

Experiments on diluted suspensions of colloidal Brownian particles have shown that the degree of correlation exhibits some fluctuations even in the absence of dynamic heterogeneity [22]. As it will be shown in detail, these fluctuations are due to statistical noise stemming from the finite number of speckles in the CCD images. In order to exploit quantitatively TRC data it is thus necessary to separate the contribution to the fluctuations of c_I due to the noise from that due to dynamic heterogeneity. Although in most cases it is not possible to directly correct the TRC time series for the noise, we will show that it is possible to correct statistical quantities derived from the TRC data and used to quantify the fluctuations of c_I. We focus in particular on three statistical objects: the time variance of $c_I(t,\tau)$, the probability distribution function (PDF) of $c_I(t,\tau)$ for a fixed τ, and the time autocorrelation of the $c_I(t,\tau)$ trace itself.

The variance of $c_I, \sigma^2_{c_I}(\tau)$, is the lowest moment of the data that provides information on the fluctuations. It corresponds to the so-called dynamical susceptibility χ_4 studied in many simulation and theoretical works on glassy systems [27–30]. In a typical simulation, χ_4 is the variance of the intermediate scattering function, or a similar correlation function describing the system's change in configuration, which is obtained from several independent runs. Similarly, $\sigma^2_{c_I}$ quantifies the fluctuations of the intensity correlation function as the system evolves through statistically independent configurations. Importantly, $\sigma^2_{c_I}$ allows one to relate temporal dynamic heterogeneity to spatial correlations of the dynamics. In fact, it can be shown that χ_4 is the volume integral of the spatial correlation of the local dynamics [31]. Therefore, large values of $\sigma^2_{c_I}$ will be indicative of long-range correlations of the dynamics. Intuitively, one can expect the variance of the fluctuations of the dynamics to scale as the inverse number of "dynamically independent" regions in the scattering volume, and thus to increase as the spatial range of the correlation of the dynamics increases. Recent TRC experiments on a shaving cream foam support this simple picture [12].

The PDF of the TRC signal is the most complete statistical characterization of the dispersion of the data. Any deviation from a Gaussian shape immediately hints to heterogeneous dynamics, as suggested by experiments on a variety of systems, including colloidal gels [22,32,33], concentrated colloidal suspensions [34] and surfactant phases [35], foams [36], and granular materials [37]. Remarkably, the shape of the PDF of c_I is often strongly reminiscent of that obtained for similar quantities in theoretical and simulation work on other glassy systems. An example is provided by simulations of spin glasses, where the fluctuations of the correlation function of the spin orientation are distributed according to a generalized Gumbel PDF [38], a probability distribution characterized by an exponential tail strikingly similar to those reported for c_I in Refs. [22,32–35,37] or shown in this paper (see Figs. 8 and 11). Similar distributions are also obtained in a variety of numerical and analytical investigations of systems with heterogeneous dynamics, both at equilibrium and out-of-equilibrium [29,39–41]. Indeed, it has been proposed that the Gumbel distribution arises as a universal PDF for various quantities measured in systems with extended spatial and/or temporal correlations [42]. Clearly, in order to compare in detail and quantitatively the PDF measured in TRC experiments to those obtained analytically or by simulations it is necessary to correct the experimental data for the contribution of the measurement noise.

The variance and the PDF of c_I describe the dispersion of the data, but are insensitive to the way the fluctuations are distributed in time. By contrast, the time autocorrelation of the TRC signal, which was introduced in Ref. [35] and which we shall term "second correlation," provides information on the temporal organization of the fluctuations of the dynamics, and sheds light on the rate and lifetime of rearrangement events. The second correlation introduced here is similar to the fourth order intensity correlation function proposed by Lemieux and Durian [43,44] and to the multitime correlation functions measured in nuclear magnetic resonance experiments probing dynamical heterogeneity near the glass transition [45]. Moreover, we note that the second correlation is the analogous, in the time domain, of the so-called second spectrum originally introduced to investigate non-Gaussian fluctuations in the dynamics of spin glasses [46].

In this paper, we first describe how to optimize a TRC measurement by correcting the CCD data for the dark noise, due to the electronic noise of the CCD, and for the uneven illumination of the detector (Sec. II). We then turn to the temporal fluctuations of c_I and analyze separately the contribution of the measurement noise, due to the finite number of pixels (Sec. III) and that due to heterogeneous dynamics (Sec. IV). We illustrate our analysis by showing TRC data obtained mainly from a dilute suspension of Brownian particles and a shaving cream foam, two model systems that exhibit homogeneous and heterogeneous dynamics, respectively. We then introduce a method for correcting the experimentally measured variance and PDF of c_I for the noise con-

tribution. The method consists of an extrapolation scheme based on the observation that the measurement noise vanishes in the limit $N \to \infty$ (N being the number of CCD pixels used to calculate c_I), whereas the fluctuations due to dynamical heterogeneities are independent of N. In Sec. V we introduce the second correlation and provide a working formula for correcting it for the noise contribution. Possible artifacts that may affect the fluctuations of c_I and lead to spurious contributions to its PDF and to the second correlation are discussed in Sec. VI, together with methods to detect or correct them. In the concluding section, we briefly discuss the connections between TRC and other techniques that measure dynamical heterogeneities in soft glassy systems, focussing on the advantages and the limitations of the various methods.

II. TIME RESOLVED CORRELATION: MEASURING THE TIME-DEPENDENT DEGREE OF CORRELATION $c_I(t,\tau)$

In a TRC experiment [22] a CCD camera is used to record, at constant rate, the speckle pattern of the light scattered by the sample [14]. The CCD images are stored on the hard disk of a personal computer (PC) for later processing. The degree of correlation c_I between speckle patterns at times t and $t+\tau$ is then calculated according to

$$c_I(t,\tau) = \frac{G_2(t,\tau)}{I(t)I(t+\tau)} - 1, \tag{1}$$

where $G_2(t,\tau)=\langle I_p(t)I_p(t+\tau)\rangle_p$ and $I(t)=\langle I_p(t)\rangle_p$, with $I_p(t)$ the intensity measured at time t by the pth CCD pixel and $\langle\cdots\rangle_p$ an average over N pixels. Note that the normalization factor in Eq. (1), $I(t)I(t+\tau)$, allows us to cancel out exactly any fluctuations due to changes in the laser power. For stationary dynamics, the intensity correlation function usually measured in a light scattering experiment $g_2(\tau)$ may be obtained from $g_2(\tau)-1=\overline{c_I(t,\tau)}$.

In Eq. (1) the intensity value at each pixel is required. In practice, however, the images recorded by the CCD are affected by a pixel- and time-dependent dark (or electronic) noise $D_p(t)$ and, possibly, by the nonuniform illumination of the detector, depending on the setup optics. To account for these effects, we write the raw signal for pixel p S_p as $S_p(t)=I_p(t)b_p/\langle b_p\rangle_p+D_p(t)$, where b_p is a time independent, spatially slowly varying function that accounts for nonuniform illumination and $\langle b_p\rangle_p$ is introduced so that the factor multiplying $I_p(t)$ has unit average. Prior to each measurement, we collect 100 dark images by covering the CCD detector with a black cap. These dark images are used to calculate the time-averaged dark noise $\overline{D_p}$. The raw signal is corrected by subtracting, pixel by pixel, the average dark noise. To estimate b_p, we average over time the dark-noise-corrected CCD signal: $b_p=\overline{S_p(t)-D_p}$. For experiments whose duration T_{exp} is much longer than the relaxation time of $g_2(\tau)$, τ_0, this procedure averages out the spatial fluctuations associated with the speckles and leads to a smooth function b_p, since for each pixel the intensity fully fluctuates many times and its time average is a good estimator of the mean intensity at a given location of the CCD detector. By contrast, when $T_{\text{exp}} \lesssim \tau_0$, b_p keeps some memory of the speckled appearance of the instantaneous intensity distribution. In this case, we further smooth b_p by averaging it over a few adjacent pixels. The desired intensity to be used in Eq. (1) is obtained from

$$I_p(t) = [S_p(t) - \overline{D_p}]\langle b_p\rangle_p/b_p. \tag{2}$$

Note that $I_p(t)$ is still affected by an instanteneous noise $\epsilon_p(t)=D_p(t)-\overline{D_p}$, since only the average dark noise could be subtracted. By definition, $\overline{\epsilon_p}=0$, while the standard deviation σ_ϵ of ϵ is typically of the order of $1/100$ of the saturation level for an eight-bit CCD camera. When all the relevant time scales of the dynamics are much longer than the inverse CCD rate, $\epsilon_p(t)$ may be considerably reduced by averaging $I_p(t)$ over a few CCD images before applying Eq. (1). In the following, we will disregard $\epsilon_p(t)$, unless when explicitly stated.

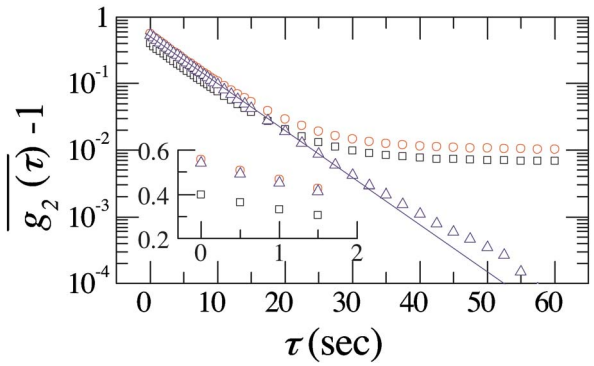

FIG. 1. (Color online) Semilogarithmic plot of the intensity time autocorrelation function measured for a suspension of monodisperse Brownian particles in the single scattering regime ($\theta=45°$). Data are averaged over $N=151\,800$ pixels and over $T_{\text{exp}}=10\,800$. Squares: intensity autocorrelation function calculated from the CCD raw signal $S_p(t)$; circles: the same data after correcting for the dark noise only; triangles: after correcting for both the dark noise and the uneven detector illumination. The line is a fit to the corrected data by a single exponential decay, the functional form of $\overline{g_2}-1$ predicted for monodisperse Brownian particles, yielding a characteristic time $\tau_0=5.8$. Inset: zoom of the small τ behavior of the intensity autocorrelation function.

We show in Fig. 1 how the different corrections discussed above affect the intensity autocorrelation function measured for a dilute suspension of monodisperse Brownian particles. Data are collected in the single scattering geometry, at a scattering angle $\theta=45°$. The particles are polystyrene spheres of radius $a=265$ nm, suspended at a volume fraction $\phi=3.7\times10^{-5}$ in almost pure glycerine cooled at 15 °C in order to make the dynamics slow enough to match the limited acquisition rate of the CCD, which is 2 Hz in this experiment. Both the dark noise and the nonuniform illumination result in a spurious increase of the base line of the autocorrelation function (squares and circles in Fig. 1) and lead to a change of its $\tau \to 0$ intercept (see inset). However, the relaxation time obtained from the small τ behavior of the intensity autocorrelation function is essentially unaffected by the dark noise and the nonuniform illumination. When the

CCD signal is corrected according to Eq. (2) (up triangles), a single exponential decay is observed, as predicted for monodisperse Brownian particles. For the corrected data, the base line is limited only by the dark noise $\epsilon_p(t)$: its value is of the order of 2×10^{-4} and is comparable to that obtained in traditional light scattering setups, which use a photomultiplier tube or an avalanche photodiode as a detector.

III. TEMPORAL FLUCTUATIONS OF $c_I(t,\tau)$: THE NOISE CONTRIBUTION

When disregarding the fluctuations of $\epsilon_p(t)$, the temporal fluctuations of the degree of correlation $c_I(t,\tau)$ at a fixed lag τ have only two independent sources: the statistical noise due to the finite number of speckles probed in the experiment and the intrinsic fluctuations of the sample dynamics. The first contribution is always present: we shall refer to it as to the "measurement noise," not to be confused with the dark noise discussed in Sec. II. The second contribution, on the contrary, is present only if the dynamics is temporally heterogeneous and thus represents the physically valuable information that we aim to extract from the fluctuations of c_I. To highlight the two different contributions, we rewrite Eq. (1) as

$$c_I(t,\tau) = g_2[a_1(t),\ldots,a_k(t);\tau] - 1 + n(t,\tau), \tag{3}$$

where $n(t,\tau)$ is the measurement noise, with $\overline{n(t,\tau)}=0$, and $g_2[a_1(t),\ldots,a_k(t);\tau]-1$ is the pixel-averaged two-time intensity correlation function that would be measured in the absence of any noise, i.e., if c_I was averaged over an infinite number of speckles. $a_1(t),\ldots,a_k(t)$ are parameters that fluctuate with time if the dynamics are heterogeneous, but are constant for homogeneous dynamics.

To illustrate this point, let us consider as an example of homogeneous dynamics the single scattering measurement of the dynamics of monodisperse Brownian particles at a scattering vector q. If the temperature is carefully controlled, the diffusion coefficient D of the particles does not evolve with time and $g_2[a_1(t),\ldots,a_k(t);\tau]-1=a_1\exp(-a_2\tau)$, with $a_1=\beta$ and $a_2=2q^2D$ constant [13]. In this case, the fluctuations of c_I are due only to the noise $n(t,\tau)$. By contrast, the spatially and temporally localized bubble rearrangements in a shaving cream foam provide a simple example of heterogeneous dynamics. For a foam, the average intensity correlation function measured in a DWS experiment in the transmission geometry has a shape very close to that for Brownian particles in single scattering: $\overline{g_2(\tau)}-1=\beta\exp[-(2\bar{\gamma}\tau)^{\bar{\mu}}]$, with $\bar{\mu}\approx0.9$ and $\bar{\gamma}=\bar{R}r^3L^2/l^{*2}$ [47,48]. Here, $\bar{R}$ is the average bubble rearrangement rate per unit time and unit volume, r^3 is the typical volume that is rearranged by a single event, L is the sample thickness, and l^* is the photon transport mean free path. In contrast with the Brownian suspension, however, the degree of correlation measured for a foam fluctuates not only because of the noise, but also because the instantaneous rearrangement rate continuously changes due to the intermittent nature of the bubble dynamics [12,36]. Hence, for the foam $g_2[a_1(t),\ldots,a_k(t);\tau]-1=a_1\exp-[a_2(t)\tau]^{a_3(t)}$, with $a_1=\beta$ const while $a_2(t)=R(t)r^3L^2/l^{*2}$ and $a_3(t)=\mu(t)$ fluctuate with time.

In view of the correction scheme described in Secs. IV and V, it is useful to first analyze the contribution to the fluctuations of c_I due to the noise. We assume that the sample dynamics be temporally homogeneous and stationary, as for the dilute suspension of Brownian particles discussed above. In this case, the parameters $a_1,\ldots,a_k$ in Eq. (3) are constant and the fluctuations of c_I are due only to the noise term $n(t,\tau)$. Since $c_I(t,\tau)$ is averaged over a large number of pixels (typically $N\gtrsim10\,000$), its temporal fluctuations at a fixed τ are expected to be Gaussian distributed, because of the central limit theorem (see Appendix B). Accordingly, only $\overline{c_I}$ and the variance $\sigma_n^2(\tau)$ of the noise $n(t,\tau)$ are needed to obtain the full probability distribution of c_I: $P_{c_I}(c_I)=(2\pi\sigma_n^2)^{-1/2}\exp[-(c_I-\overline{c_I})^2/2\sigma_n^2]$. For homogeneous dynamics, $\sigma_n^2(\tau)=\sigma_{c_I}^2(\tau)\equiv\overline{c_I(t,\tau)^2}-\overline{c_I(t,\tau)}^2$. To calculate $\sigma_{c_I}^2$, we recall that the variance of a quantity y that depends on the m variables $x_1,\ldots,x_m$ is given by

$$\sigma_y^2=\sum_{i=1}^{m}\left[\frac{\partial y}{\partial x_i}\right]^2_{x_i=\overline{x_i}}\sigma_{x_i}^2+\sum_{i\neq j}\left[\frac{\partial y}{\partial x_i}\frac{\partial y}{\partial x_j}\right]_{\substack{x_i=\overline{x_i}\\ x_j=\overline{x_j}}}\sigma_{x_i,x_j}, \tag{4}$$

where $\sigma_{x_i}^2\equiv\overline{x_i^2}-\overline{x_i}^2$ is the variance of x_i and $\sigma_{x_i,x_j}\equiv\overline{x_ix_j}-\overline{x_i}\,\overline{x_j}$ is the covariance between x_i and x_j $(i\neq j)$. The first sum accounts for the sensitivity of y to the fluctuations of the independent variables $x_1,\ldots,x_m$, while the second sum accounts for any correlations between the x_i's. If distinct x_i's are uncorrelated, $\overline{x_ix_j}=\overline{x_i}\,\overline{x_j}$ for $i\neq j$ and the second sum vanishes.

By applying Eq. (4) to the definition of c_I, Eq. (1), we find

$$\sigma_{c_I}^2(\tau)=1/\bar{I}^4\sigma_{G_2}^2(\tau)+2\overline{G_2(\tau)}^2/\bar{I}^6\sigma_I^2+2\overline{G_2(\tau)}^2/\bar{I}^6\sigma_{I,J}(\tau)-4\overline{G_2(\tau)}/\bar{I}^5\sigma_{G_2,I}(\tau), \tag{5}$$

where we have introduced the notation $J(t)\equiv I(t+\tau)$. In writing Eq. (5) we have used $\bar{I}=\bar{J}$ and $\sigma_{G_2,I}=\sigma_{G_2,J}$, because the scattered light was assumed to be stationary.

The physical origin of the fluctuations of I and G_2, quantified by σ_I^2 and $\sigma_{G_2}^2$, as well as that of the correlation between I and J and between I and G_2, quantified by $\sigma_{I,J}$ and $\sigma_{G_2,I}$ is the finite number of pixels over which the instantaneous intensity and the intensity correlation are averaged. To illustrate this point, let us consider as an example $I(t)$. As the sample evolves through different configurations, the speckle pattern fluctuates with a characteristic time τ_0. Since the instantaneous pixel-averaged intensity is calculated for a finite set of speckles, different speckle patterns yield slightly different values of $I(t)$. The larger the number of the sampled speckles, the closer will $I(t)$ be to the "true" value of the average scattered intensity, whose estimator is $\bar{I}$, and thus the smaller will be σ_I^2. Indeed, we show in Appendix A that $\sigma_I^2\sim N^{-1}$, as expected from the central limit theorem. Moreover, one expects the instantaneous pixel-averaged intensity at time t to be correlated to the same quantity measured at time $t+\tau$, at least for $\tau\lesssim\tau_0$, because it takes a few τ_0 for the speckle pattern to be completely renewed. Therefore, the covariance term $\sigma_{I,J}(\tau)$ will vanish only for $\tau\gg\tau_0$. More pre-

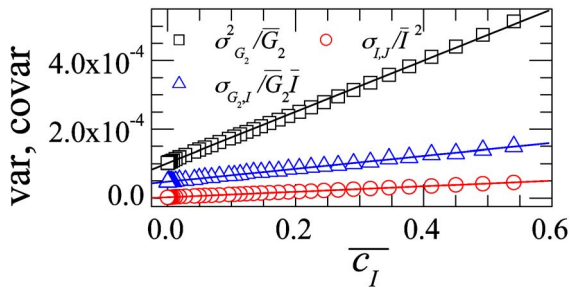

FIG. 2. (Color online) Parametric plot of the normalized variance and covariance terms in the RHS of Eq. (5), as a function of $\overline{c_I(\tau)}$, for the same experiment as in Fig. 1. The lines are linear fits to the data, suggesting the c_I dependence of Eq. (6).

cisely, we expect $\sigma_{I,J}(\tau)$ to be proportional to $\overline{G_2(\tau)}$. In fact, $\sigma_{I,J}(\tau)$ is precisely the un-normalized correlation function measured by using the whole CCD chip as a single detector, similarly to the case of a traditional light scattering experiment where the detector collects a large number of speckles.

Similar arguments may be invoked for $\sigma^2_{G_2}(\tau)$ and $\sigma_{G_2,I}(\tau)$, suggesting that the variance and covariance factors in Eq. (5) scale with N^{-1} and depend linearly on the average correlation function

$$\sigma_{x_i,x_j}(\tau) = N^{-1}[A_{x_i,x_j} + B_{x_i,x_j}\overline{c_I(\tau)}], \tag{6}$$

where x_i and x_j stand for any of I, J, and G_2, while A_{x_i,x_j} and B_{x_i,x_j} are constants whose values are given in Appendix A. To test the linear dependence of the variance and covariance factors on the time-averaged correlation function, we plot parametrically $\sigma^2_{G_2}(\tau), \sigma_{I,J}(\tau)$, and $\sigma_{G_2,I}(\tau)$ as a function of $\overline{c_I(\tau)}$, for data obtained in the single scattering experiment on Brownian particles, as shown in Fig. 2. In all cases the data are very well fitted by straight lines, thus confirming the validity of Eq. (6).

The τ dependence of the variance of the measurement noise can be obtained by substituting Eq. (6) into Eq. (5). Using $\overline{G_2(\tau)} = \bar{I}^2[\overline{c_I(\tau)}+1]$ (see Appendix B), one finds a third order polynomial dependence of the variance of $n(t,\tau)$ on $\overline{c_I(\tau)}$:

$$\sigma^2_n(\tau) = \sigma^2_{c_I}(\tau) = N^{-1}\sum_{l=0}^{3} \alpha_l \overline{c_I(\tau)}^l, \tag{7}$$

where the coefficients α_l can be obtained from $\bar{I}$, A_{x_i,x_j}, and B_{x_i,x_j}. Note that this third-order polynomial dependence is due to the choice of the normalization of c_I [see Eq. (1)]. If the denominator was chosen to be $\bar{I}^2$, as in traditional light scattering experiments, only the first term in the right-hand side (RHS) of Eq. (5) would be nonzero and $\sigma^2_{c_I}(\tau) \propto \sigma^2_{G_2}$, i.e., the fluctuations would increase linearly with $\overline{c_I(\tau)}$. Although the normalization we have chosen leads to a more complicated expression for $\sigma^2_n(\tau)$, we remind that it suppresses spurious variations of c_I due to fluctuations of the incoming beam power and thus should be used in TRC experiments. The inset of Fig. 3 shows a semilogarithmic plot of $\sigma_{c_I}(\tau)$ vs

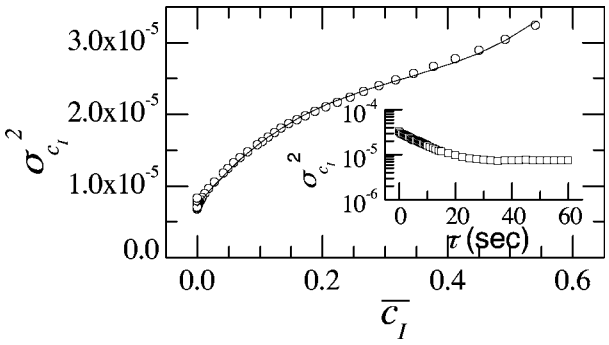

FIG. 3. Main plot: parametric representation of the variance of c_I as a function of $\overline{c_I(\tau)}$ for the same experiment as in Figs. 1 and 2 (single scattering from a dilute suspension of Brownian particles). The line is a fit of Eq. (7) to the data. Inset: same data plotted vs τ.

τ for the Brownian particles, confirming that the noise of c_I decreases with τ, as indicated by Eq. (7). In the main plot, the same data are plotted parametrically as a function of $\overline{c_I(\tau)}$. A very good agreement is found between the experimental data and the polynomial form suggested by Eq. (7), as shown by the line.

The N^{-1} dependence of $\sigma^2_n(\tau)$ is the key feature that will be exploited in the correction for the measurement noise. To test this scaling, we analyze the time series of speckle images recorded for the Brownian particle suspension, for which $\sigma^2_{c_I} = \sigma^2_n$, by processing different number of pixels. First, all pixels of each image are processed and $c_I(t,\tau)$ and its variance $\sigma^2_{c_I}(\tau)$ are calculated. Each image is then divided into two regions of interest (ROI) of equal size. For each ROI, c_I and its variance are calculated and the values of $\sigma^2_{c_I}(\tau)$ obtained for the two ROIs are averaged, yielding the variance of c_I when only $N/2$ pixels are processed. This scheme is iterated until the size of each ROI is reduced to 225 pixels. Figure 4 shows $\sigma^2_{c_I}(\tau)$ as a function of the inverse number of processed pixels N^{-1} for three time delays corresponding to 0.09, 0.87, and 8.7 times the relaxation time of g_2-1, respectively. In all cases, the data for $N^{-1} < 1.2\times10^{-4}$ are very well fitted by a straight line that goes through the origin, as shown in the inset [49]. This confirms that for temporally homogeneous dynamics $\sigma^2_{c_I} \propto N^{-1}$, as indicated by Eq. (7). Note that

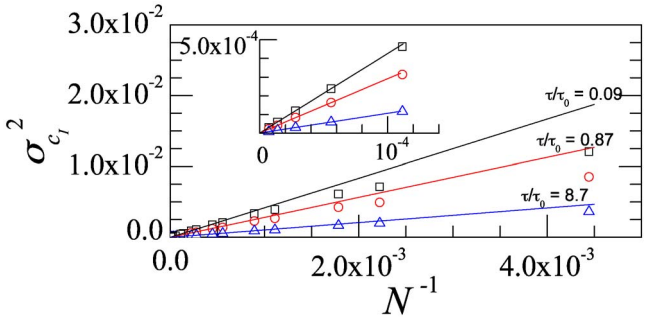

FIG. 4. (Color online) For the same experiment on Brownian particles as in the preceding figures: variance of c_I as a function of the inverse number of pixels over which c_I is averaged. The lines are linear fits to the data for $N^{-1} \leq 1.2\times10^{-4}$, demonstrating that for large N $\sigma^2_{c_I} \propto N^{-1}$. The inset zooms in the region near to the origin.

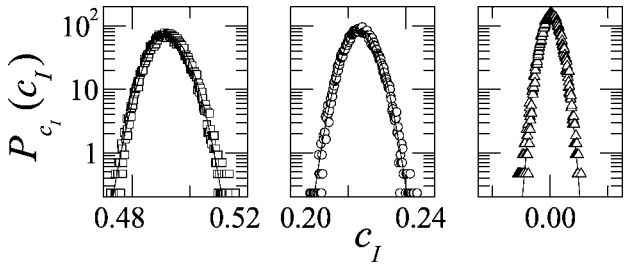

FIG. 5. Symbols: PDF of $c_I(t,\tau)$, $P_{c_I}(c_I)$, for the same suspension of Brownian particles as for the preceding figures. From left to right, the normalized delay τ/τ_0 is 0.09, 0.87, and 8.7. In the three panels the c_I axis spans an interval of equal width (0.04). The lines are Gaussian distributions whose mean and standard deviations are directly obtained from the c_I time series, without any fitting parameter.

a deviation from this linear trend is observed at the largest N^{-1}, due to edge effects. In fact, the contribution of each pixel to c_I is not completely independent from that of nearby pixels, because the intensity of the speckle pattern is spatially correlated over a distance of a few pixels. Pixels far from the edges of a ROI have more nearby pixels than those on the edges; accordingly, the statistically independent contribution to c_I carried by a bulk pixel is less than that of an edge pixel. When reducing the size of the processed ROI, the weight of edge pixels relative to bulk pixels increases and corrections to the N^{-1} scaling become increasingly apparent. These corrections are negligible for $N \gtrsim 8000$, as seen in Fig. 4. We find that a similar N^{-1} scaling is obtained at all time delays (data not shown). Indeed, the slopes of the straight line fits to $\sigma^2_{c_I}$ vs N^{-1} provide an estimate of the proportionality coefficient $\Sigma_{l=0}^{3}\alpha_l\overline{c_I(\tau)}^l$ that agrees within 1% with the value directly obtained when calculating $\sigma^2_{c_I}$ by processing the maximum number of available pixels.

For temporally homogeneous dynamics, the statistics of the variables $G_2(t,\tau)$ and $I(t)$ in Eq. (1) is Gaussian, because of the central limit theorem. As a consequence, the probability density function (PDF) of c_I is also Gaussian, as demonstrated in Appendix B. In Fig. 5 we show the PDF of c_I for various τ for a Brownian suspension of particles. The symbols are the experimental data, while the lines are Gaussian PDFs with mean $\overline{c_I(\tau)}$ and standard deviation $\sigma_{c_I}(\tau)$ obtained directly from the c_I time series, without any fitting parameters. An excellent agreement between the data and the theoretical shape of the distributions is observed at all τ.

IV. TEMPORALLY HETEROGENEOUS DYNAMICS: CORRECTIONS FOR THE NOISE CONTRIBUTION

In temporally heterogeneous dynamics, the fluctuations of c_I are due both to the noise and to dynamical heterogeneity. In this section we propose a method for correcting the variance and the PDF of c_I for the noise contribution, so as to obtain the statistics of the fluctuations due to dynamical heterogeneity. Moreover, we show that in some instances the full temporal evolution of c_I may be corrected for the noise, thus allowing $g_2(t,\tau)-1$ to be determined, not only its variance and PDF.

A. Correction of the variance of c_I

In the case of dynamically heterogeneous processes, the parameters $a_1,\ldots,a_k$ in the two-time correlation function $g_2[a_1(t),\ldots,a_k(t);\tau]-1$, Eq. (3), fluctuate with t. Therefore, an extra term σ_{g_2} contributes to the variance of c_I, in addition to the noise term analyzed in the preceding section:

$$\sigma^2_{c_I}(\tau) = N^{-1}\sum_{l=0}^{3}\alpha_l\overline{c_I(\tau)}^l + \sigma^2_{g_2}(\tau). \tag{8}$$

In writing the expression above, we have assumed that no correlation exists between the noise $n(t,\tau)$ due to the finite number of pixels and the fluctuations of $a_1,\ldots,a_k$. Using Eq. (4), $\sigma^2_{g_2}$ may be expressed as

$$\sigma^2_{g_2}(\tau) = \sum_{i=1}^{k}\left[\frac{\partial g_2}{\partial a_i}\right]^2_{a_i=\overline{a_i}}\sigma^2_{a_i} + \sum_{i\neq j}\left[\frac{\partial g_2}{\partial a_i}\frac{\partial g_2}{\partial a_j}\right]_{\substack{a_i=\overline{a_i}\\ a_j=\overline{a_j}}}\sigma_{a_i,a_j}. \tag{9}$$

An example where $\sigma^2_{g_2}$ assumes a particularly simple form is given by the dynamics of a shaving cream foam, resulting from intermittent bubble rearrangements, as measured in a DWS experiment. We find that the fluctuations in the instantaneous decay rate $\gamma(t)$ of the correlation function are slow compared to $\overline{\gamma}$, so that at any given time g_2-1 is well approximated by a stretched exponential $\beta\exp[-(\gamma(t)\tau)^{\mu(t)}]$. Small variations of $\mu(t)$ account for slight changes of the decay rate on a time scale comparable to $\overline{\gamma}^{-1}$. For example, if the dynamics tend to slow down during the measurement of g_2-1, the initial decay of the correlation function will be faster than its final decay. Thus, the shape of g_2 will be more stretched than the average one ($\mu<\overline{\mu}$). Conversely, $\mu>\overline{\mu}$ if the dynamics accelerate during the measurement of g_2-1. By taking into account the fluctuations of both γ and μ, Eq. (9) yields, for the foam,

$$\sigma^2_{g_2}(\tau) = (\overline{\gamma}\tau)^2\beta^2\exp[-2(\overline{\gamma}\tau)^{\overline{\mu}}]\left\{\left(\frac{\overline{\mu}}{\overline{\gamma}}\sigma_\gamma\right)^2 + [\ln(\overline{\gamma}\tau)\sigma_\mu]^2\right\} \tag{10}$$

with $\sigma^2_\gamma=\overline{(\gamma-\overline{\gamma})^2}$ and $\sigma^2_\mu=\overline{(\mu-\overline{\mu})^2}$. Equation (10) extends a similar expression given in Ref. [12], where only the fluctuations of γ where taken into account. However, here we still neglect possible correlations between γ and μ that could be described by including the second term of the RHS of Eq. (9).

A direct test of Eq. (10) is not possible, since we experimentally only access $\sigma^2_{c_I}$, not $\sigma^2_{g_2}$. Therefore, for the foam as well as for the general case of temporally heterogeneous dynamics it is desirable to subtract the trivial contribution of the measurement noise from the experimentally measured $\sigma^2_{c_I}$, in order to obtain the physically relevant variance $\sigma^2_{g_2}$. We have tested two different approaches. In the first method, the linear dependence of σ_{x_i,x_j} on $\overline{c_I}$ shown in Fig. 2 is used to derive formulas for these quantities that are independent of the instantaneous dynamics and thus of the homogeneous vs heterogeneous nature of the dynamics. These formulas are presented in Appendix A. Unfortunately, although they provide separately fairly good estimates of the various terms

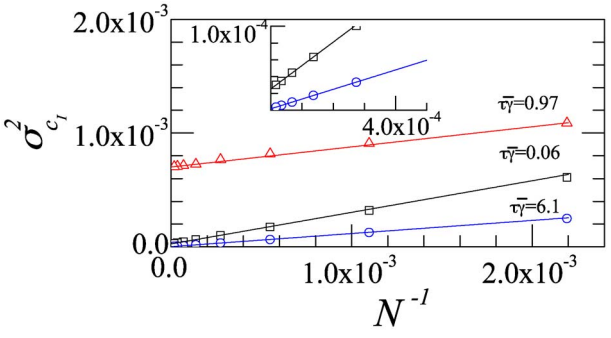

FIG. 6. (Color online) Variance of $c_I(t,\tau)$ for a foam, as a function of the inverse number of pixels over which c_I is averaged, for three time delays τ. The lines are linear fits to the data for $N^{-1} < 5.5\times10^{-4}$. For $\tau\bar{\gamma}\approx 1$, the intercept of the fit strongly departs from zero, indicating temporarily heterogeneous dynamics as discussed in the text. Note that the fit yields a nonzero intercept also at small delay, as shown in the inset that zooms into the small $\sigma^2_{c_I}$, large N region. Data were collected in the DWS transmission geometry for a duration $T_{\rm exp}=160$ s, 242 times longer than the relaxation time of c_I, $\bar{\gamma}^{-1}=0.33$ s.

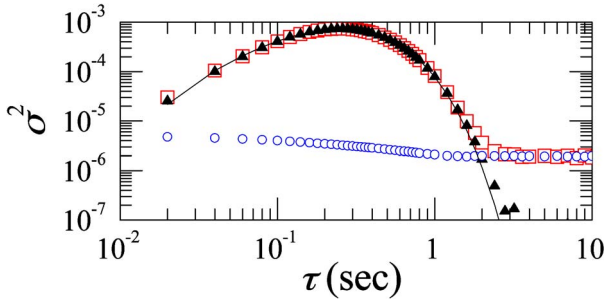

FIG. 7. (Color online) Variance of $c_I(t,\tau)$ for a foam, as a function of τ. Open squares: variance of the raw data (c_I); open circles: noise contribution; solid triangles: $\sigma^2_{g_2}(\tau)$, the contribution due to the fluctuations of the number of rearrangement events per unit time. The line is a fit to $\sigma^2_{g_2}(\tau)$ using Eq. (10). Data were collected in the DWS transmission geometry.

σ_{x_i,x_j}, when combined using Eq. (5) to evaluate σ^2_n uncertainties add up leading to errors of the order of 30–40 %, as tested on the data for the single scattering experiment on the Brownian particles.

In the following, we describe in detail a second method that has proven to be highly effective. The key point is to recognize that, contrary to the noise term, the fluctuations of $g_2(a_1,\ldots,a_k;\tau)$ do not depend on the number of pixels over which c_I is averaged. This is because in the far field geometry of the scattering experiments described in this work, each CCD pixel collects light scattered by the whole illuminated sample. Thus, any spatial or temporal heterogeneity of the dynamics affects in the same way the signal measured by each pixel. The different pixel-number dependence of the noise and the fluctuations [first and second term in the RHS of Eq. (8), respectively] suggests a way to discriminate between these two contributions. We analyze the speckle images by processing different number of pixels, as described for the Brownian suspension in Sec. III, and plot $\sigma^2_{c_I}(\tau)$ as a function of N^{-1}, as shown in Fig. 6. As indicated by Eq. (8), the slope of a linear fit to the data yields $\Sigma^3_{l=0}\alpha_l\overline{c_I(\tau)^l}$, while the intercept at $N^{-1}=0$ is $\sigma^2_{g_2}(\tau)$, the desired variance of the correlation function due to dynamical heterogeneity. Thus, the representation of Figs. 4 and 6 allows one to extrapolate $\sigma^2_{c_I}$ to $N=\infty$, where the measurement noise vanishes. As seen in the inset of Fig. 6, for $\tau\bar{\gamma}\ll 1$ or $\tau\bar{\gamma}\gg 1$ the intercept of the linear fit is very close to zero, indicating that at these delays the fluctuations of c_I are mainly determined by the measurement noise. By contrast, at intermediate delays the intercept clearly departs from zero, revealing the intermittent nature of the dynamics of the foam.

In Fig. 7 we plot the τ dependence of $\sigma^2_{c_I}$ measured for the foam, together with the noise contribution $\sigma^2_n = N^{-1}\Sigma^3_{l=0}\alpha_l\overline{c_I(\tau)^l}$ and that of the intrinsic fluctuations $\sigma^2_{g_2}$. The noise contribution is extracted from the slope of $\sigma^2_{c_I}$ vs N^{-1}, while the variance of the intrinsic fluctuations is given by the $N^{-1}\to 0$ limit of $\sigma^2_{c_I}$ vs N^{-1}. At all τ we find $\sigma^2_{c_I}=\sigma^2_n+\sigma^2_{g_2}$ within 0.8 %, thus confirming that our analysis allows us to correctly account for the two contributions to the fluctuations of c_I. Note that, while the shape of the time-averaged correlation function $\overline{g_2}-1$ is almost the same for the foam and the Brownian particles (a slightly stretched exponential for the former and a simple exponential decay for the latter), the τ dependence of the fluctuations of c_I is very different (compare the inset of Fig. 3 with Fig. 7), thus allowing temporally heterogeneous dynamics to be unambiguously detected. For the foam, correcting $\sigma^2_{c_I}$ for the noise contribution is especially important at time delays far from the mean relaxation time, because the intrinsic fluctuations die off for $\tau\to 0$, when virtually no rearrangement had a chance to occur, and for $\tau\to\infty$, when so many rearrangement events occurred that the statistical fluctuations of their number are negligible. By contrast, we recall that σ^2_n remains finite at all τ. Once corrected for the noise contribution, $\sigma^2_{g_2}(\tau)$ is very well described by Eq. (10), as shown by the line in Fig. 7. Interestingly, the fluctuations are maximal on the time scale of the mean relaxation time, a general feature found also in the dynamic susceptibility χ_4 measured in simulations. Intuitively, this can be explained by recognizing that the correlation function is most sensitive to a change of the instantaneous relaxation time for $\tau\approx\tau_0$. Finally, note that when comparing the absolute values of $\sigma^2_{g_2}(\tau)$ and χ_4 one should keep in mind that the latter is usually defined as the variance of the correlation function multiplied by the number M of particles in the system. Therefore, for homogeneous dynamics $\chi_4\sim 1$, since the variance of the number fluctuations is of order $1/M$, while $\chi_4>1$ for heterogeneous dynamics. In the case of the foam shown in Fig. 7, taking M as the number of bubbles in the scattering volume leads to $M\sigma^2_{g_2}(\tau)\sim 1000$, indicating strongly heterogeneous dynamics.

B. Correction of the PDF of c_I

In the absence of intrinsic dynamical fluctuations, knowledge of the average degree of correlation $\overline{c_I}$ and of the noise variance σ^2_n is sufficient to fully determine the PDF of c_I at

fixed lag, because c_I is a Gaussian variable. Heterogeneous dynamical processes, on the contrary, lead in general to non-Gaussian distributions of $c_I(t,\tau)$ [22,32,35], whose shape depends on both the dynamical process and the time delay τ. Because $c_I(t,\tau)$ is the sum of two uncorrelated random variables, $g_2[a_1(t),\ldots,a_k(t);\tau]-1$ and the noise $n(t,\tau)$, the PDF of c_I is the convolution of the probability distribution of $g_2[a_1(t),\ldots,a_k(t);\tau]-1$ with that of $n(t,\tau)$ [50]:

$$P_{c_I}(c_I) = P_{g_2-1}(g_2-1) \otimes P_n(n), \tag{11}$$

where $P_x(x)$ denotes the PDF of x and $(f\otimes g)(x) = \int dx' f(x')g(x-x')$ is the convolution product. In order to recover the physically relevant PDF of g_2-1 from the measured $P_{c_I}(c_I)$, one may use standard Fourier transform techniques to deconvolute the experimental data, using $P_n(n)$ as the response function [51]: $P_{g_2-1}=\mathcal{F}^{-1}[\mathcal{F}(P_{c_I})/\mathcal{F}(P_n)]$, where $\mathcal{F}$ and $\mathcal{F}^{-1}$ indicate direct and inverse Fourier transform, respectively. Unfortunately, this procedure is very sensitive to noise in the data and leads typically to unstable solutions exhibiting wide oscillations. Instead, we use a technique similar to the indirect Fourier transformation (IFT) method used to process static scattering data. Details on the IFT method can be found in Refs. [52,53], here we simply describe the main steps of our implementation. We first assume that the unknown PDF of g_2-1 at fixed lag τ may be written as the linear superposition of a set of suitable functions ϕ_k:

$$P_{g_2-1} = \sum_{k=1}^{M} \mu_k \phi_k(g_2-1). \tag{12}$$

It is convenient to choose $\phi_k(x)=\mathrm{rect}(x-x_k;2\Delta)$, where

$$\mathrm{rect}(x-x_k;2\Delta) = \begin{cases} 1: & |x-x_k| \leqslant \Delta, \\ 0: & \text{elsewhere} \end{cases} \tag{13}$$

is a square pulse of width 2Δ centered on x_k. 2Δ is taken to be the width of the bins used to calculate the PDF of c_I, i.e., the separation between the c_I coordinates of the M experimental P_{c_I} data. Because the convolution is a linear transformation, Eqs. (11) and (12) yield the following guess for the PDF of c_I:

$$\begin{aligned} P_{\mathrm{guess}}(c_I) &= \sum_{k=1}^{M} \mu_k \mathrm{rect}(c_I - c_{I,k};2\Delta) \otimes P_n(c_I) \\ &= \sum_{i=k}^{M} \frac{\mu_k}{2}[\mathrm{erf}(x^+) - \mathrm{erf}(x^-)] \end{aligned} \tag{14}$$

with

$$x^{\pm} = \frac{1}{\sqrt{2}\sigma_n}(c_I - c_{I,k} \pm \Delta). \tag{15}$$

Here $\mathrm{erf}(x)=2\pi^{-1/2}\int_0^x \exp(-u^2)du$ is the error function [50] and $c_{I,k}$ is the center of the kth bin used to calculate the experimental PDF. In writing the last line of Eq. (14) we have used $P_n(c_I)=(2\pi\sigma_n^2)^{-1/2}\exp[-c_I^2/2\sigma_n^2]$ and calculated explicitly the convolution product. We note that the width of the rect functions is typically much smaller than that of the Gaussian noise P_n, so that the difference of the erf functions in square brackets is very close to a Gaussian. We stress that the only unknowns in Eqs. (14) and (15) are the coefficients μ_k, since the variance of the noise σ_n^2 can be obtained directly from the experimental c_I using the extrapolation scheme described in the preceding subsection.

In principle, the coefficients μ_k can be determined by fitting Eq. (14) to the experimentally measured PDF of c_I. Once the μ_k's are known, the desired PDF of g_2-1 can be obtained by using Eq. (12). In practice, two issues must be addressed when determining the set of μ_k. First, noise in the experimental P_{c_I} can make the fitting procedure unstable. It is therefore convenient to smooth the experimental P_{c_I} before fitting it by Eq. (14). To this end, P_{c_I} is approximated by a smooth curve P_{sm} obtained by fitting the data by a suitable function. We find that in most cases

$$P_{\mathrm{sm}}(c_I) = A e^{\nu_1(c_I-c_0)+\nu_2(c_I-c_0)^2-\nu_3\exp[\nu_4(c_I-c_0)]} \tag{16}$$

fits the whole experimental PDF well, although fitting P_{c_I} piecewise may be sometimes necessary. Note that the Gumbell PDF corresponds to the case $\nu_1=\nu_4=\alpha>0$, $\nu_2=0$, and $\nu_3=1$ [38]. The coefficients μ_k are then found by fitting $P_{\mathrm{guess}}(c_I)$ to P_{sm}, rather than directly to P_{c_I}. Second, the PDF of g_2-1 determined by inserting the μ_k's thus obtained in Eq. (14) often exhibits large oscillations. This is because the erf functions in Eq. (14) do not form an orthogonal basis, as discussed in Ref. [53]. This problem can be solved by adding a stabilization condition when fitting P_{sm} by P_{guess}. We follow Ref. [53] and determine the set of μ_k by minimizing the following expression:

$$\sum_{l=1}^{L} [P_{\mathrm{sm}}(c_{I,l}) - P_{\mathrm{guess}}(c_{I,l})]^2 + \Lambda \sum_{k=1}^{M-1} (\mu_{k+1}-\mu_k)^2. \tag{17}$$

The first term in the above expression corresponds to the usual sum of squared deviations between the fitting function (P_{guess}) and the data (P_{sm}). The second term assigns a cost to any large variation between successive μ_k and thus tends to suppress all fast oscillation of P_{guess}. The relative weight of the two terms is controlled by the Lagrange multiplier Λ, whose optimum value is determined as described in Ref. [53].

The top panel of Fig. 8 shows the PDF of c_I measured in the DWS TRC experiment on foam, for $\tau=0.02$ s (open circles). The solid line is the smoothed PDF, P_{sm}, obtained by fitting the data to Eq. (16). The dotted line is the Gaussian PDF of the noise P_n whose width is σ_n (for display purposes, P_n has been centered on c_I, rather than on 0). In the bottom panel, the thick line is the PDF corrected for the noise contribution P_{g_2-1}. Note that the right wing of the corrected PDF drops much more abruptly than that of the raw data (for comparison, the uncorrected and the smoothed PDF are also plotted in the bottom panel). The left wing, on the contrary, is almost unaffected by the correction. This is a consequence of the nearly exponential behavior of the left wing: indeed, it can be shown that the convolution of an exponential function with a Gaussian is again exponential, with the same growth rate. We test how close the raw data and the corrected PDF

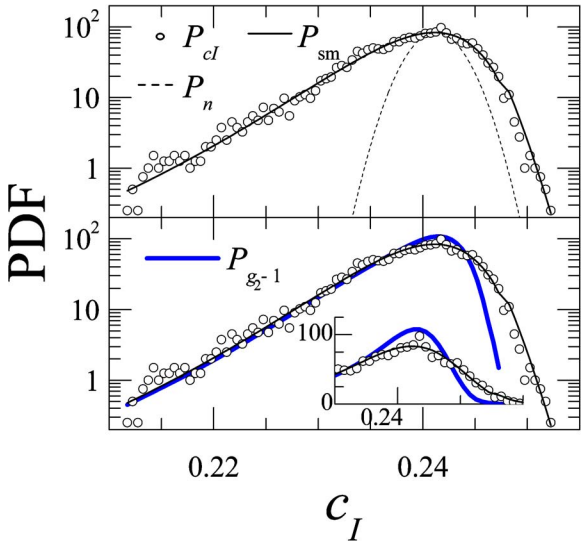

FIG. 8. (Color online) Top panel: PDF of $c_I(t,\tau)$ for a foam, for τ=0.2 sec (open circles); data were in the DWS transmission geometry. The continuous line is the smoothed distribution $P_{\rm sm}$ obtained from a fit to Eq. (16). The dotted line is the Gaussian PDF of the noise. Bottom panel: the corrected distribution P_{g_2-1} (thick line), together with the raw data and the smoothed PDF (same symbols as in the top panel). Note the much steeper decay of the right wing of the corrected PDF. The inset shows the data around the peak in a linear axis graph.

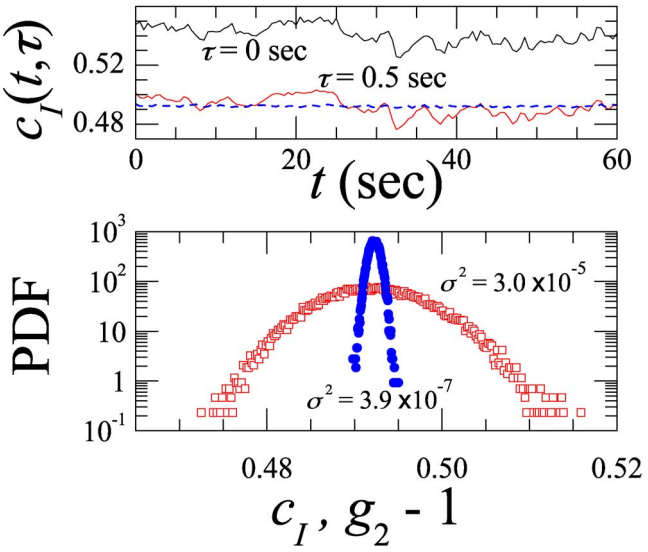

FIG. 9. (Color online) Top panel: $c_I(t,0)$ and $c_I(t,\tau_1=0.5\ \text{sec})$ measured for a diluted suspension of Brownian particles, for which the relaxation time of g_2-1 is τ_0=5.8. Data are plotted over a short time window to show the strong correlation between the two traces. The dashed blue line is $g_2(t,\tau_1)-1$ obtained by correcting $c_I(t,\tau_1)$ for the noise contribution according to Eq. (19): the fluctuations due to the noise are almost completely removed. Bottom panel: PDF of $c_I(t,\tau_1)$ (open squares) and of $g_2(t,\tau_1)-1$ (solid circles), obtained over the full duration of the experiment ($T_{\rm exp}$=10800 s). The PDFs are labeled by their variance.

are to a Gumbel distribution by fitting the data to the expression of Eq. (16), with $\nu_2=0$ and $\nu_1=\nu_3\nu_4$, corresponding to a generalized Gumbel PDF [38]. For the raw data, we find $\nu_3=1.04$, very close to $\nu_3=1$, the value for a Gumbel PDF. By contrast, for the corrected data $\nu_3=0.42$, showing that the right wing of the corrected PDF strongly departs from both a Gumbel distribution and the "universal" PDF of Ref. [42], for which $\nu_3=\pi/2\approx1.57$. A more detailed investigation of the shape of the PDF of c_I for various delays τ and different systems will be presented elsewhere: here we just stress the importance of the noise correction in view of any quantitative comparison.

C. Direct correction of $c_I(t,\tau)$ for $\tau\ll\tau_0$

The methods developed in Secs. IV A and IV B allow one to calculate the variance and the PDF of g_2-1, but not to correct directly the time-dependent degree of correlation $c_I(t,\tau)$. Here we show that such a correction is possible, i.e., that the noise-free $g_2(t,\tau)-1$ at fixed τ may be retrieved as a function of t, provided that the following assumptions are fullfilled: (i) the dynamics is homogeneous on a time scale comparable to the CCD exposure time and (ii) $\tau\ll\tau_0$, where τ_0 is the average relaxation time of g_2-1.

We first observe that $c_I(t,\tau=0)$ measures the so-called contrast of the speckle pattern, or coherence factor β. The latter is determined only by the speckle-to-pixel size ratio, which is a time-independent quantity, and by the blurring due to the fluctuations of the speckle during the time the CCD chip is exposed [14]. If (i) is fulfilled, the amount of blurring is constant over time and hence $c_I(t,0)$ fluctuates only because of the noise [54]. Therefore, $n(t,0)$ can be directly obtained from the experimentally measured $c_I(t,0)$:

$$n(t,0)=c_I(t,0)-\overline{c_I(t,0)}. \tag{18}$$

If in addition (ii) is also fulfilled, $n(t,\tau)\approx n(t,0)$, because the noise evolves on the same time scale as the speckle pattern, τ_0. Indeed, by analyzing TRC data for Brownian particles, we have shown in Ref. [35] that the noise is highly correlated for $\tau\ll\tau_0$. This suggests that $c_I(t,\tau)$ may be directly corrected according to $g_2(t,\tau)-1=c_I(t,\tau)-n(t,\tau)\approx c_I(t,\tau)-n(t,0)$, with $n(t,0)$ obtained via Eq. (18). This approximation may be further refined by taking $n(t,\tau)\approx[n(t,0)+n(t+\tau,0)]/2$ rather than $n(t,\tau)\approx n(t,0)$ and by scaling this estimate of the noise so that its standard deviation matches the actual standard deviation of $n(t,\tau)$:

$$g_2(t,\tau)-1=c_I(t,\tau)-[\sigma_n(\tau)/\sigma_n(0)][n(t,0)+n(t+\tau,0)]/2\sigma_n. \tag{19}$$

Here, the standard deviation of the noise of $c_I(t,\tau)$, $\sigma_n(\tau)$, is obtained by applying the extrapolation scheme described in Sec. IV A, while $n(t,0)$ and $n(t+\tau,0)$ are given by Eq. (18) and $\sigma_n(0)$ is directly calculated from $n(t,0)$.

We test Eq. (19) on TRC data taken for the dilute suspension of Brownian particles, for which the fluctuations of c_I are due only to the measurement noise: $c_I(t,\tau)=n(t,\tau)+\overline{c_I(t,\tau)}$. The top panel of Fig. 9 shows a portion of $c_I(t,0)$ and $c_I(t,\tau_1)$, with $\tau_1=0.5\ \text{s}\ll\tau_0=5.8$ s. Clearly, the two traces are highly correlated, as expected if $n(t,\tau_1)$

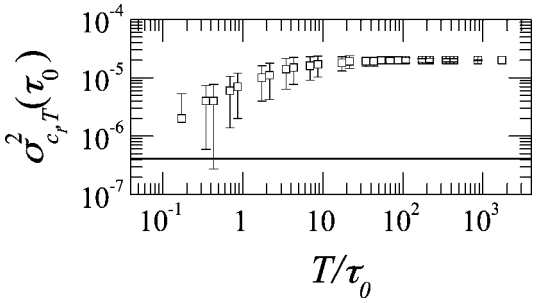

FIG. 10. Variance of $c_I(t,\tau=\tau_0)$ calculated over a duration T as a function of T normalized by the mean relaxation time τ_0, for a suspension of Brownian particles. A similar behavior is observed for all τ. The line is the contribution to the variance of $c_I(t,\tau=\tau_0)$ of the CCD electronic noise (see the text for more details).

$\approx n(t,0)$. The dotted line is $g_2(t,\tau_1)-1$ calculated according to Eq. (19). Notice that $g_2(t,\tau_1)-1$ is almost constant, as expected for temporally homogeneous dynamics, thus demonstrating the effectiveness of the correction. The bottom panel shows the PDF of $c_I(t,\tau_1)$ and $g_2(t,\tau_1)-1$ calculated over the whole duration of the experiment. By correcting $c_I(t,\tau_1)$ for the noise, its variance is reduced by almost a factor of 100 (from 3.0×10^{-5} to 3.9×10^{-7}). The residual fluctuations of $g_2(t,\tau_1)$ are most likely due to the noise $\epsilon_p(t)$ discussed in reference to Eq. (2), whose variance we estimate to be of the order of 3.9×10^{-7} [55].

D. Influence of the duration of the experiment

The analysis of the fluctuations of c_I presented in Secs. IV A and IV B was developed under the assumption that the dynamics be stationary, so that data could be collected over a period $T_{\rm exp}$, much longer than the average relaxation time of the intensity correlation function τ_0. Dynamical heterogeneity, however, appear to be more prominent for systems close to jamming or quenched in an out-of-equilibrium state. For these systems, meeting the condition $T_{\rm exp}\gg\tau_0$ is often impossible, since the sample may be aging, leading to nonstationary dynamics, or because, even if the dynamics is stationary, the relaxation time may be as large as several tens of hours. It is therefore important to address the issue of the influence of the experiment duration on the measured σ_{c_I}.

Let us first consider the simpler case of homogeneous dynamics. We divide the time series of $c_I(t,\tau)$ obtained for the Brownian particles into non-overlapping segments of duration $T<T_{\rm exp}$. We denote by $\sigma^2_{c_I,T}(\tau)$ the mean value of the variance of $c_I(t,\tau)$ calculated for each segment of duration T, and plot in Fig. 10 $\sigma^2_{c_I,T}$ as a function of T normalized by the relaxation time τ_0 (the data refer to $\tau=\tau_0$, a similar behavior is observed for all τ). For $T/\tau_0\gg1$, $\sigma^2_{c_I,T}$ is independent of T, because in this regime the experiment duration is long enough for the system (and thus the speckle pattern) to sample a sufficiently large number of different configurations. Consequently, $\sigma^2_{c_I,T}$ saturates to the maximum value given by Eq. (7), which is dictated only by τ and the number of CCD pixels. Note that for T/τ_0 close to one $(T/\tau_0=0.87)$, $\sigma^2_{c_I,T}$ is still significantly lower than its saturation value (about 35%), while it increases to 95% for $T/\tau_0>20$ and saturates only for $T/\tau_0\geqslant50$. As T/τ_0 decreases below 1, the amplitude of the fluctuations is significantly reduced when decreasing T, since the system is not given enough time to explore significantly different configurations. For $T/\tau_0\ll1$, the speckle pattern is essentially frozen on the time scale of the experiment duration: the fluctuations of c_I due to the evolution of the speckle pattern are thus expected to be almost completely suppressed. For the data shown in Fig. 10, this regime is not quite reached, since the CCD acquisition rate could not be fast enough to allow for several images to be acquired on a time scale much smaller than τ_0 (the smallest lag between images is 0.5 s$=\tau_0/11.6$). In the $T/\tau_0\to0$ regime, the main contribution to $\sigma^2_{c_I,T}$ should come from the CCD electronic noise $\epsilon_p(t)$, whose variance, σ^2_ϵ, is shown as a line in Fig. 10. The data shown in this figure clearly demonstrate that care must be taken when comparing the fluctuations measured in experiments whose relative duration $T_{\rm exp}/\tau_0$ is different.

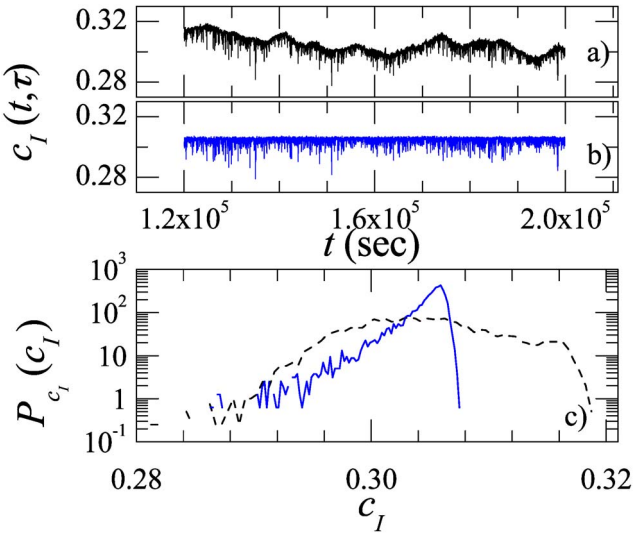

FIG. 11. (Color online) (a) Time variation of c_I for a multilamellar vesicle gel, for $\tau=100$ s. The mean relaxation time is $\tau_0=5050$ s, the duration of the experiment is $T=80\,000$ $s=15.8\times\tau_0$. (a) Raw data; (b) the same data after applying the correction Eq. (19), (c): PDF of the traces shown in (a) (dotted line) and (b) (solid line).

For heterogeneous dynamics, we expect the behavior of $\sigma^2_{c_I,T}$ to be qualitatively similar, although the situation will be in general more complicated. In fact, in this case the relevant time scales to which $T_{\rm exp}$ has to be compared are not only the mean relaxation time of $g_2-1\tau_0$, but also the characteristic time of the "intrinsic" fluctuations of the dynamics, described by the variation of the parameters $a_1(t),\ldots,a_k(t)$ in Eq. (3). As an example, for the foam data shown in Figs. 6 and 7 $\tau_0=\overline{\gamma(t)}^{-1}=0.32$ s, while the temporal fluctuations of the decay rate occur on a much longer time scale $\tau_{\rm fluct}\approx7$ s [36] (see also Fig. 13 below and the associated discussion). Hence, in order to measure precisely the fluctuations the experiment should last more than about $20\tau_{\rm fluct}$, rather than just $20\tau_0$. For other jammed materials, on the contrary, the intrinsic fluctuations may be much faster than

τ_0, as demonstrated by the sudden sharp drops of c_I resulting from intermittent rearrangements in a closely packed multilamellar vesicle system [56], shown in Fig. 11(a). In this case, at least for the smallest time lags, the analysis proposed in Sec. IV C allows the slow fluctuations due to the measurement noise to be suppressed, while preserving the fast drops of c_I that contain the physically relevant information on the dynamical intermittency, as seen in Fig. 11(b). Note the dramatic change of the shape of the PDF of c_I before and after correcting the data, as shown in Fig. 11(c).

V. THE SECOND CORRELATION

In the previous sections, the fluctuations of c_I were analyzed in terms of their variance and PDF. Additional information on the system dynamics can be obtained by studying not only the probability distribution of the fluctuations and its second moment, but also the way these fluctuations occur in time. We characterize the temporal properties of c_I at a fixed lag τ by introducing the time autocorrelation function of $c_I(t,\tau)$:

$$C_{c_I}(\Delta t,\tau)=\frac{\overline{c_I(t,\tau)c_I(t+\Delta t,\tau)}-\bar{c}_I^2}{\overline{c_I(t,\tau)^2}-\bar{c}_I^2}. \tag{20}$$

With this choice of the normalization, $C_{c_I}(0,\tau)=1$, and $C_{c_I}(\Delta t,\tau)=0$ if $c_I(t,\tau)$ and $c_I(t+\Delta t,\tau)$ are uncorrelated (e.g., for $\Delta t\to\infty$). Because C_{c_I} is the correlation function of a time-varying quantity $c_I(t,\tau)$ which is obtained itself by correlating the scattered intensity, we shall term it the "second correlation," in analogy with the "second spectrum" first introduced in the context of spin glasses [46]. The second spectrum describes in the frequency domain the fluctuations around the mean value of the spectrum of a time-dependent quantity. Similarly, the second correlation describes—in the time domain—the fluctuations of the degree of correlation between the time-dependent system configurations. The second correlation is also similar to the fourth order intensity correlation function introduced in Refs. [43,44], $g_T^{(4)}(\tau)=\overline{I(0)I(T)I(\tau)I(\tau+T)}/\bar{I}^4$. Note, however, that $g_T^{(4)}(\tau)$ compares the scattered intensity, and thus the sample configuration, at four successive times, while the second correlation compares the *change* in sample configuration occurring over two time intervals of duration τ separated by a time Δt.

As for the case of the PDF discussed in Sec. IV, the second correlation contains contributions from both the physically relevant intrinsic fluctuations of $g_2[a_1(t),\ldots,a_k(t);\tau]-1$ and the noise $n(t,\tau)$. We focus on stationary dynamics measured over a period $T_{\rm exp}\gg\tau_0$ and assume that the fluctuations of $g_2[a_1(t),\ldots,a_k(t);\tau]-1$ and $n(t,\tau)$ are uncorrelated: $\overline{g_2 n}=g_2\bar{n}$ for all Δt. Under these assumptions and by using Eq. (3), Eq. (20) yields

$$C_{c_I}(\Delta t,\tau)=\frac{\sigma_{g_2}^2(\tau)C_{g_2}(\Delta t,\tau)+\sigma_n^2(\tau)C_n(\Delta t,\tau)}{\sigma_{g_2}^2(\tau)+\sigma_n^2(\tau)}, \tag{21}$$

where C_{g_2} and C_n are the correlation functions of the fluctuations of g_2 and n, respectively, defined similarly to Eq. (20). Experiments on Brownian particles (homogeneous dynamics) show that $C_n(\Delta t,\tau)\simeq\overline{c_I}(\Delta t)/\beta$ for all τ [35]. Indeed, C_n is expected to be proportional to c_I because the τ dependence of the noise time autocorrelation stems from the same physical mechanism leading to the decay of the intensity correlation function, i.e., the renewal of the speckle pattern over time discussed in Sec. III. In order to extract the desired second correlation of g_2 from the noise-affected C_{c_I}, we use a method similar to the extrapolation technique adopted for the calculation of the variance of g_2. At Δt and τ fixed, C_{c_I} depends on the number N of processed pixels through the σ_n^2 term in Eq. (21) We omit for simplicity the explicit dependence on Δt and τ and insert Eq. (7) into Eq. (21):

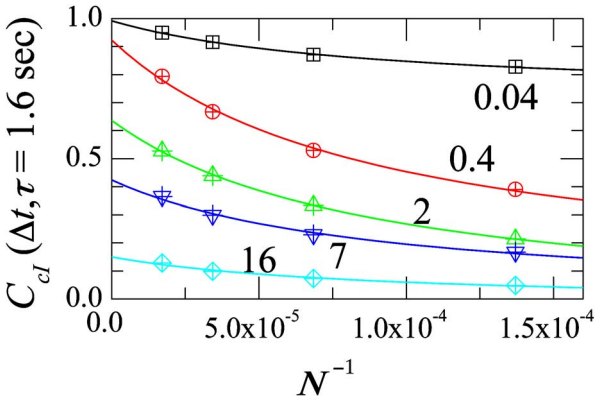

FIG. 12. (Color online) Correction method for C_{g_2}. Symbols: the second correlation C_{c_I} as a function of the inverse number of processed pixels, for various Δt (shown by the labels, in s) and for $\tau=1.6$ s (only the data for the largest N are shown). The data are obtained from a DWS measurement on a foam. The lines are fits to the data using Eq. (22); the full range of the fit is shown in the figure. The outcome of the fit are the values of $C_{g_2}(\Delta t,\tau)$ and $C_n(\Delta t,\tau)$ shown with the same symbols in Fig. 13.

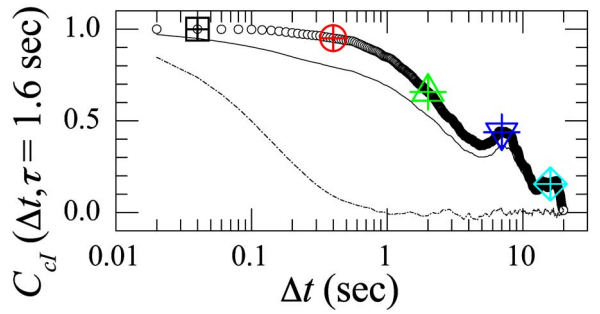

FIG. 13. (Color online) Time autocorrelation function of the fluctuations of g_2 for a foam, obtained from the second correlation $C_{c_I}(\Delta t,\tau)$ by applying the correcting scheme described in the text. Small open circles: the noise-free C_{g_2-1}; solid line: the experimentally measured C_{c_I}; dashed line: the noise contribution, C_n. The large symbols are the values of C_{g_2-1} obtained from the fit to the corresponding data shown in Fig. 12. Note the peaks of C_{g_2-1} at $\Delta t\approx 7$ s, and $\Delta t\approx 14$ s, suggesting pseudoperiodic rearrangement events, as discussed in the text.

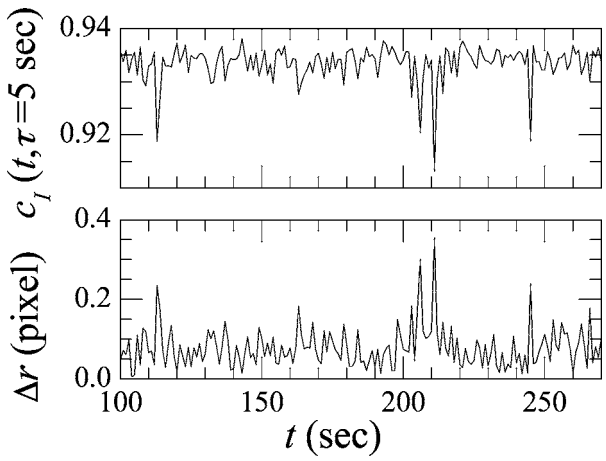

FIG. 14. Top panel: $c_I(t,\tau)$ measured for a static scatterer, a ground glass, for $\tau=5$ s. Note the sharp drops of the degree of correlation that greatly exceed the noise of the data. Bottom panel: rigid displacement between the pair of speckle images used to calculate $c_I(t,\tau)$ above, measured by PIV. The sharp drops of c_I are artifacts due to larger-than-average rigid shifts of the speckle images.

$$C_{c_I}(N) = \frac{\sigma_{g_2}^2 C_{g_2} + C_n N^{-1} \sum_{l=0}^{3} \alpha_l \overline{c_I^l}}{\sigma_{g_2}^2 + N^{-1} \sum_{l=0}^{3} \alpha_l \overline{c_I^l}} \tag{22}$$

The LHS of this expression can be calculated by processing ROIs of the speckle images of different sizes, as explained in Secs. III and IV, and plotted as a function of N^{-1}, as shown in Fig. 12 for a foam. The RHS of Eq. (22) is then used as a fitting function for $C_{c_I}(N)$, where the fitting parameters are the desired C_{g_2} and C_n, while $\sigma_{g_2}^2$ and $\Sigma_{l=0}^3 \alpha_l \overline{c_I^l}$ are obtained independently from the correction of the variance of c_I, as explained in Sec. IV A.

By repeating this procedure for all Δt and τ of interest, the full second correlation can be corrected for the noise contribution. We show in Fig. 13 $C_{g_2}(\Delta t,\tau)$ for a foam (open circles), together with the uncorrected data (C_{c_I}, solid line) and the noise contribution (C_n, dashed line). Remarkably, a peak is visible in C_{g_2}, at $\Delta t=\Delta t^* \approx 7$ *s*. Note that the peak is not present in C_n, whose only relevant time scale is that of the relaxation of $\overline{c_I}$, $\overline{\gamma}^{-1}=0.32$ s. Therefore, the peak in C_{g_2} must be associated with the intrinsic fluctuations of the dynamics due to the intermittent bubble rearrangements. Indeed, the peak indicates that the fluctuations of the instantaneous decay rate $\gamma(t)$ are pseudoperiodic on a time scale of the order of Δt^*. We are currently investigating the origin of this feature.

VI. POSSIBLE ATRIFACTS

In a TRC measurement, the focus is on the fluctuations of the degree of correlation, rather than on its mean value. As a consequence, TRC measurements are very sensitive to various sources of spurious fluctuations, whose effects are usually less prominent or even negligible in traditional dynamic light scattering experiments, since they tend to average out. An example is provided in the top panel of Fig. 14, which shows c_I measured for the speckle pattern generated in the transmission geometry by a ground glass, a scatterer whose dynamics are completely frozen in. In this case, we would expect c_I to fluctuate slightly only because of the electronic noise $\epsilon_p(t)$ discussed in Sec. II. Surprisingly, sharp drops of the degree of correlation are clearly visible. Because the drops are rare, they do not affect significantly $\overline{c_I}$; however, they do change significantly the PDF of c_I and the second correlation. Indeed, one would mistakenly take the dynamics to be intermittent, if the sample was not known. The origin of this artifact is the laser beam pointing instability. Beam pointing instability is the characteristic noise of lasers that results in small fluctuations of the propagation direction of the output beam. Since the speckle pattern is centered around the propagation direction, any change of the incoming beam direction entails a rigid shift of the speckle image with respect to the CCD detector. Thus, the intensity at each pixel slightly changes, leading to a drop of c_I. To demonstrate that this mechanism is indeed responsible for the sharp drops of c_I observed in Fig. 14, we show in the bottom panel the corresponding shift $\Delta r(t,\tau)$ between pairs of images taken at time t and $t+\tau$, measured by particle imaging velocimetry (PIV) [57]. This method is based on spatial cross-correlation techniques and allows the rigid motion between two images to be quantified with subpixel resolution (our adaption of PIV to speckle imaging will be described elsewhere). A comparison between the two panels of Fig. 14 clearly shows that the anomalously large drops of c_I are due to larger-than-average rigid shifts of the speckle images. Note that shifts as small as a fraction of pixel, corresponding to a few microns, have a measurable impact on c_I.

This example shows how sensitive to instabilities TRC is. Therefore, care must be taken in order to minimize possible instabilities and to identify any spurious fluctuations of c_I. Moreover, attempts should be done to correct c_I for artifacts. In our experience, the most common artifact encountered in TRC experiments is similar to that exemplified by Fig. 14: fluctuations or sharp drops of c_I due to a rigid shift of the speckle pattern, rather than to the characteristic "boiling" or flickering of the speckle images associated with the evolution of the sample configuration. In addition to beam pointing instability, temperature variations are often to blame for spurious features in the temporal evolution of c_I.

Temperature variations may change the direction of propagation of light because of refractive effects, since the refractive index n_D varies with temperature T. As an example, let us consider a typical small-angle single scattering measurement on an aqueous sample contained in a rectangular cell, whose entrance and exit walls are perpendicular to the incoming beam. Light scattered at an angle θ_s equal to, e.g., 15 ° is refracted at the water-to-air interface and exits at an angle given by Snell's law: $\theta_{air}=\arcsin(n_D \sin\theta_s)$ [58]. A temperature fluctuation δT induces a variation $\delta\theta_{air}$ given by

$$\delta\theta_{\text{air}} = \frac{\partial\theta_{\text{air}}}{\partial n_D}\frac{\partial n_D}{\partial T}\delta T = \frac{\sin\theta_s\,\partial n_D/\partial T}{\sqrt{1-\sin^2\theta_s n_D^2}}\delta T \approx 2.8\times 10^{-5}\ \text{rad}, \tag{23}$$

where we have used $n_{\text{D}}=1.33$, $\partial n_{\text{D}}/\partial T \approx 10^{-4}\ \text{K}^{-1}$ for water and we have taken $\delta T=1$ K. In a typical small angle setup the sample-to-CCD distance is at least 10 cm and the pixel size is about 10 μm, resulting in a shift of the speckle associated to the direction θ_{s} of the order of 0.28 pixels, sufficient to significantly reduce c_I. Thus temperature fluctuations of the order of 1 K may lead to measurable spurious fluctuations of c_I because of refractive effects.

In most single scattering wide-angle apparatuses the sample cell is cylindrical and both the incoming beam and the scattered light cross all optical interfaces at normal incidence, so that refractive effects are avoided. Nevertheless, any change of the refractive index due to temperature variations would still result in a change of the speckle pattern. This is because each speckle is associated to a well defined value of the scattering vector $\mathbf{q}_s$. If n_D changes, the scattering angle θ_{s} corresponding to $\mathbf{q}_s$ is modified, since $\theta_s = 2\arcsin(\lambda_0 q_s/4\pi n_D)$, where λ_0 is the laser in-vacuo wavelength. Accordingly, the speckle pattern is contracted or dilated around the $q=0$ direction. This is the same effect as the radial shift of the speckle pattern when changing the wavelength of the incident radiation, which was studied in the 1970 [59]. When only a limited portion of the speckle pattern corresponding to a small solid angle is imaged on the CCD detector (as it is the case, e.g., for the single scattering experiments at $\theta=45°$ reported in this paper), such a global contraction or dilation results, locally, in a rigid shift of the speckles. The change $\delta\theta_s$ of θ_s in response to a temperature fluctuation δT is

$$\begin{aligned}\delta\theta_{\text{s}} &= \frac{\partial\theta_{\text{s}}}{\partial n_{\text{D}}}\frac{\partial n_{\text{D}}}{\partial T}\delta T \\ &= \frac{-2\lambda_0 q_s\,\partial n_D/\partial T}{n_D\sqrt{16\pi^2 n_D^2+\lambda_0^2 q_s^2}}\delta T \\ &\approx -6.2\times 10^{-5}\ \text{rad},\end{aligned} \tag{24}$$

where we have used $n_D=1.33$, $\lambda_0=0.535$ μm, $q_s=12.44$ $\mu\text{m}^{-1}(\theta_s=45°)$, $\partial n_D/\partial T \approx 10^{-4}\ \text{K}^{-1}$, and $\delta T=1$ K. Taking the sample-to-CCD distance to be 10 cm, we find that a fluctuation $\delta T=1$ K would result in a shift of the speckle pattern of 6.2 μm, comparable to the pixel size. This would lead to a catastrophic drop of c_I, since the speckle size is typically of the order of the pixel size. Indeed, even a fluctuation ten times smaller, $\delta T=0.1$ K, would have a measurable impact on c_I. Similar arguments apply also to multiple scattering experiments. Note that DWS experiments are more sensitive to variations of n_D than single scattering measurements are, because minute changes of q at each scattering event add up along the photon path, eventually resulting in a significant change of the phase of scattered photons.

Various strategies are possible to avoid the artifacts discussed above, or at least to mitigate their effects on TRC data. The impact of beam pointing instability can be minimized by reducing as much as possible the light path between the laser and the sample, or by delivering the beam via fiber optics. In the latter case, beam pointing instability results in fluctuations of the laser-to-fiber coupling efficiency and thus of the incident intensity, I_{in}. Because c_I is normalized with respect to the instantaneous pixel-averaged intensity [see Eq. (1)], fluctuations of I_{in} have little if any effect. Temperature should be controlled at least to within 0.1 K and the sample or sample holder temperature should be monitored, so that any suspect feature in c_I could be compared to the temperature record. A PIV analysis similar to that presented in Fig. 14 is a useful test to check whether a spurious rigid shift of the speckle pattern is at the origin of large drops of c_I.

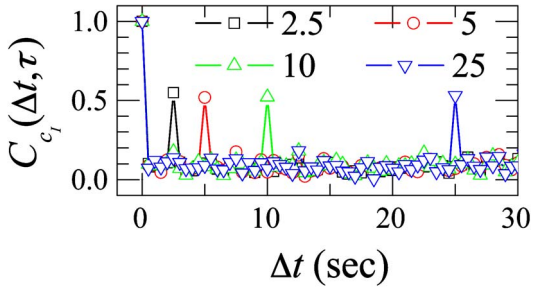

FIG. 15. (Color online) Second correlation measured for a perfectly frozen speckle pattern. The curves are labeled by τ, in s. Note the spurious peaks at $\Delta t=\tau$, due to the CCD dark noise, as discussed in the text.

The input from PIV measurements may also be used to correct for the effect of a rigid shift $\Delta\mathbf{r}$ of the speckle pattern. This could be achieved by constructing a corrected speckle image, shifting back by $-\Delta\mathbf{r}$ the second image of the pair used to compute c_I. The corrected image would then be used to calculate c_I. Standard image-processing techniques [60] can be used to obtain subpixel shifts. Alternatively, one may exploit the fact that in the presence of both a rigid shift $\Delta\mathbf{r}$ and a genuine evolution of the speckle pattern, the measured degree of correlation $c_{I,\text{meas}}$ factorizes as $c_{I,\text{meas}}(t,\tau)=c_I(t,\tau)[g_{2,\text{sp}}(\Delta\mathbf{r})-1]$ (a proof is given in the Appendix of Ref. [17]). Here $g_{2,\text{sp}}(\Delta\mathbf{r})-1$ is the normalized spatial autocorrelation function of the speckle image and $c_I(t,\tau)$ is the degree of correlation that would be measured in the absence of any shift. We are currently exploring both approaches.

We conclude this section by reporting a spurious feature due to the electronic noise ϵ_p, which may affect the second correlation $C_{c_I}(\Delta t,\tau)$ measured for time lags τ much smaller than the typical relaxation time. On those short time scales, the speckle pattern is essentially frozen; therefore, we shall use as an example the series of images of a perfectly frozen speckle pattern obtained as described at the end of Sec. IV C. We process the data as usual and calculate the variance of c_I. For all lags $\tau>0$ the same value is obtained, which is taken as an estimate of σ_ϵ^2. This has the advantage of excluding other artifacts, such as a possible rigid shift of the speckle pattern. As shown in Fig. 15, the second correlation exhibits spikes at $\Delta t=\tau$, emerging from a baseline close to zero. This is a spurious effect due to the fact that the electronic noise ϵ_p is delta correlated in time. Therefore, ϵ_p contributes an extra

term to $\overline{c_I(t,\tau)c_I(t+\Delta t,\tau)}$ whenever two out of the four intensity terms involved in this expression are measured at the same time, as for $\Delta t=\tau$. A rigorous calculation can be found in Ref. [36], showing that the height of the spurious peaks is 0.5, in good agreement with Fig. 15. The spikes of the second correlation shown in a figure of a (withdrawn) preprint authored by some of us [61] are most likely due to this effect.

VII. CONCLUSIONS

We have shown that TRC allows heterogeneous dynamics to be unambiguously discriminated from homogeneous dynamics. In order to quantify dynamical heterogeneity, three statistical objects are particularly insightful: the variance of c_I, which corresponds to the dynamical susceptibility χ_4, the PDF of the degree of correlation, and its time autocorrelation function—the second correlation. Statistical noise due to the finite number of pixels over which c_I is averaged can contribute significantly to the fluctuations of the degree of correlation. Thanks to the correction scheme described in this paper, the variance, PDF, and time autocorrelation of c_I can be corrected for this contribution, thus making quantitative measurements of heterogeneous dynamics accessible to scattering techniques. These corrections are particularly important when the intrinsic fluctuations are comparable to or even smaller than the noise. This may occur because dynamic heterogeneity is mild, e.g., in moderately concentrated suspensions of colloids [62], or because the number of available pixels is reduced, e.g., in a small angle light scattering or XPCS setup, where the lowest accessible q vectors correspond to small rings centered around the transmitted beam and containing a limited number of pixels [21]. Corrections are also important when comparing TRC data obtained from different apparatuses, for which both the speckle size and the number of pixels may differ, or when analyzing small angle data, since the number of pixels in the rings associated to different q vectors varies with q.

In addition to providing a quantitative description of dynamical fluctuations for systems in a stationary or quasistationary state, TRC is a useful tool for studying rapidly evolving dynamics, e.g., during gelation [36], as well as the response to an instantaneous perturbation, e.g., an applied shear [63]. Because in both cases the dynamics may evolve on time scales comparable to or even shorter than the relaxation time of g_2, a representation of the time evolution of c_I is more appropriate and insightful than that of the two-time correlation function. Limitations to the applicability of TRC are mainly due to the CCD acquisition rate, which typically does not exceed a few tens or hundreds of Hz. An additional experimental constraint is the need to store the acquired images on the hard disk of a PC and to process them at the end of the experiment: data sets up to several Gb are not infrequent.

Other techniques have been proposed in the last few years to study dynamical heterogeneity. New light scattering methods include speckle visibility spectroscopy (SVS) [64,65] and the measurement of higher order intensity correlation functions [43,44]. In a SVS experiment, one measures $c_I(t,\tau=0)$, that is the instantaneous contrast—or visibility—of the speckle pattern $\langle I_p^2(t)\rangle_p/\langle I_p(t)\rangle_p^2-1$. The contrast depends on the evolution of the speckle pattern during the exposure (integration) time of the CCD. A significant evolution on this time scale leads to a blurred speckle pattern image, and thus to a reduced contrast. Fluctuations of the contrast can therefore be related to dynamical fluctuations on the time scale of the exposure time. Because the latter is typically much shorter than the time between successive CCD acquisitions, SVS and TRC provide complementary information, on fast and slow dynamics, respectively. Note that SVS data can be obtained on the fly, with no need to store images, since only one image at a time has to be processed. Higher order intensity correlation functions [43,44], calculated by a dedicated hardware, allow one to discriminate between homogeneous and intermittent dynamics. The time scales that are probed and the required measuring time are similar to those in a traditional light scattering experiment: dynamics as fast as a fraction of μsec can be measured, but the largest available delay is limited to a few tens of seconds and the experiment duration has to be at least 1000 times longer than the largest relaxation time of the system. These constraints limit the applicability to glassy soft matter.

Video and confocal scanning microscopy have been used to study dynamical heterogeneity in concentrated colloidal suspensions [66]. Microscopy and TRC are complementary techniques: while the former provides unsurpassed details on the motion at a single particle level, scattering data typically benefit from better statistics. Additionally, scattering experiments usually require smaller particles than microscopy, a plus when dealing with very slow dynamics and when sedimentation effects should be minimized. Other techniques that can probe heterogeneous behavior in soft glasses are dielectric [67] and rheological [68] measurements whose sensitivity is pushed to the limits set by thermal fluctuations. The outcome of these experiments shares intriguing similarities with TRC data, such as the non-Gaussian distribution of voltage fluctuations in dielectric measurements on suspensions of Laponite [67]. Whether these similarities are coincidental or stem from a common physical origin remains an open question.

In the future, a deeper understanding of both spontaneous dynamical fluctuations and the response to external perturbations in soft glassy systems will likely require the combination of different techniques, possibly applied simultaneously on the same sample. We believe that TRC can play an important role in this endeavor, thanks to its ability to detect instantaneous variations in the dynamics.

ACKNOWLEDGMENTS

We thank P. Ballesta, E. Pitard, L. Berthier, P. Holdsworth, and J. P. Garrahan for many useful discussions, and D. Popovic for bringing to our attention the works on the second spectrum. This work was supported in part by the European MCRTN "Arrested matter" (Grant No. MRTN-CT-2003-504712) and the NoE "Softcomp," and by CNES (Grant No. 03/CNES/4800000123), CNRS (PICS No. 2410), Minstère de la Recherche (Grant No. ACI JC2076), and the

TABLE I. Coefficients needed to calculate the contribution of the measurement noise to $\sigma_{I,J}(\tau), \sigma^2_{G_2}(\tau)$, and $\sigma_{G_2,I}(\tau)$.

	$\tau=0$	$\tau\to\infty$
$\sigma_{I,J}(\tau)$	σ_I^2	0
$\sigma^2_{G_2}(\tau)$	$\sigma^2_{G_2(0)}$	$2\overline{I}^2\sigma_I^2$
$\sigma_{G_2,I}(\tau)$	$\sigma_{G_2(0),I}$	$\overline{I}^2\sigma_I^2$

Swiss National Science Foundation. L.C. thanks the Institut Universitaire de France for financial support.

APPENDIX A: CALCULATION OF THE VARIANCE AND COVARIANCE TERMS IN EQ. (6)

In this section we provide additional details on the two approaches to the calculation of the variance of the measurement noise mentioned in Sec. III. We first show that the variance and covariance terms in Eq. (6) may be expressed in a way that is independent of the homogeneous vs heterogeneous nature of the dynamics, and then explicitly demonstrate the N^{-1} scaling of σ_n^2 that was used in the correction scheme presented in this paper.

The quantities of interest are the variance of the pixel-averaged intensity σ_I^2, the covatiance between I and $J\sigma_{I,J}(\tau)$, the variance of the un-normalized intensity correlation function $\sigma^2_{G_2}(\tau)$, and the covariance between G_2 and $I\sigma_{G_2,I}(\tau)$. We recall that $I(t)=\langle I_p(t)\rangle_p, J(t)=\langle I_p(t+\tau)\rangle_p$ and drop in the following the explicit dependence on t in the notation of all time-varying variables. We assume the dynamics to be stationary and the experiment duration much longer than the average relaxation time of c_I. We start by noting that σ_I^2 quantifies the fluctuations of the *instantaneous* pixel-averaged intensity. Therefore, σ_I^2 is independent of the nature of the dynamics: indeed, any dynamical process that fully renews the speckle pattern will allow all possible values of I to be sampled over time and thus will lead to the same σ_I^2. In contrast, $\sigma_{I,J}(\tau)$, $\sigma^2_{G_2}(\tau)$, and $\sigma_{G_2,I}(\tau)$ depend on the way the correlation between *distinct* speckle patterns fluctuates with time and therefore contain contributions due both to the measurement noise and to the intrinsic fluctuations of the dynamics. However, note that the $\tau\to 0$ and $\tau\to\infty$ limits of these quantities are insensitive to the dynamics, because they involve either instantaneous properties of the speckle pattern (for $\tau=0$), or quantities related to pairs of speckle images totally uncorrelated (for $\tau\to\infty$). This observation, together with the linear dependence of $\sigma_{I,J}(\tau)$, $\sigma^2_{G_2}(\tau)$, and $\sigma_{G_2,I}(\tau)$ on $\overline{c_I}$ in the absence of dynamical heterogeneity shown in Fig. 2, suggests the following form for the contribution of the measurement noise to the covariance and variance terms:

$$\sigma_{I,J}(\tau)=\sigma_{I,J}(\infty)+\frac{\overline{c_I(\tau)}}{\beta}[\sigma_{I,J}(0)-\sigma_{I,J}(\infty)],$$

$$\sigma^2_{G_2}(\tau)=\sigma^2_{G_2}(\infty)+\frac{\overline{c_I(\tau)}}{\beta}[\sigma^2_{G_2}(0)-\sigma^2_{G_2}(\infty)]\sigma_{G_2,I}(\tau)=\sigma_{G_2,I}(\infty)+\frac{\overline{c_I(\tau)}}{\beta}[\sigma_{G_2,I}(0)-\sigma_{G_2,I}(\infty)]. \quad \text{(A1)}$$

All coefficients in the RHS of the above equations are not affected by dynamical heterogeneity. Table I summarizes their values in terms of quantities that can be directly obtained from the speckle images, regardless of the nature of the dynamics.

As mentioned in Sec. IV, estimates of σ_n^2 obtained by using Eq. (A1) and Table I are typically affected by a significant error. In this paper we have proposed a more robust correction method, based on the N^{-1} scaling of the measurement noise variance, which we demonstrate here. For the sake of simplicity, we assume in the following that there is no correlation between the instantaneous value of the intensity at distinct pixels, i.e., $\overline{I_pI_q}=\overline{I_p}\,\overline{I_q}$ for $p\neq q$. Physically, this corresponds to a speckle size much smaller than the pixel size; this requirement considerably simplifies the calculations, but it can be relaxed without changing the N^{-1} scaling, as we shall show at the end of this Appendix.

For experiments whose duration is much longer than the relaxation time of c_I, the intensity at any given pixel fully fluctuates many times and its probability distribution over time is the same as the instantaneous PDF of I_p calculated over all N pixels; therefore averages over time and over pixels can be swapped. We take advantage of this property and of the statistical independence between I_p and I_q to write

$$\sigma_I^2=\overline{\frac{1}{N^2}\sum_{p,q}I_pI_q}-\overline{I}^2=\frac{1}{N^2}\sum_{p=1}^{N}\overline{I_p^2}+\frac{1}{N^2}\sum_{p\neq q}\overline{I_pI_q}-\overline{I}^2. \quad \text{(A2)}$$

This expression may be further simplified by noting that moments of the intensity at any pixel are equal to those of, let us say, pixel 1: $\overline{I_p^2}=\overline{I_1^2}$ and $\overline{I_p}=\overline{I_1}=\overline{I}$. Hence

$$\sigma_I^2=\frac{1}{N}\overline{I_1^2}+\frac{N(N-1)}{N^2}\overline{I}^2-\overline{I}^2=\frac{1}{N}\overline{I_1^2}. \quad \text{(A3)}$$

Similarly, one obtains

$$\sigma^2_{I,J}=\overline{\frac{1}{N^2}\sum_{p,q}I_pJ_q}-\overline{IJ}=\frac{1}{N}\overline{G_2}+\frac{N(N-1)}{N^2}\overline{IJ}-\overline{IJ}=\frac{1}{N}\overline{c_I}\overline{I}^2, \quad \text{(A4)}$$

$$\sigma_{G_2,I}=\overline{\frac{1}{N^2}\sum_{p,q}I_pJ_pI_q}-\overline{G_2}\overline{I}=\frac{1}{N}\overline{I_1^2J_1}-\frac{1}{N}\overline{G_2}\overline{I}, \quad \text{(A5)}$$

and

$$\sigma^2_{G_2}=\overline{\frac{1}{N^2}\sum_{p,q}I_pJ_pI_qJ_q}-\overline{G_2}^2=\frac{1}{N}\overline{I_1^2J_1^2}-\frac{1}{N}\overline{G_2}^2. \quad \text{(A6)}$$

Equations (A3)–(A6) show that all the terms in the LHS of the expression of σ_n^2, Eq. (6), are indeed proportional to N^{-1}.

As a final remark, we show that the form of the equations derived above is not changed by a short-ranged correlation between the intensity of distinct pixels, such as that typically observed in the CCD speckle images. We consider, as an example, the calculation of σ_I^2; similar arguments apply also to the other variance and covariance terms. Because the spatial correlation is short-ranged, the intensity of pixel p will be correlated only to that of a small number M of nearby pixels, whereas for all other pixels $\overline{I_pI_q}\approx\overline{I_p}\,\overline{I_q}$. We indicate

the set of nearby pixels by Q_p and split the double sum over distinct pixels in Eq. (A2) as follows:

$$\frac{1}{N^2}\sum_{p\neq q}\overline{I_pI_q}=\frac{1}{N^2}\sum_{p,q\in Q_p}\overline{I_pI_q}+\frac{1}{N^2}\sum_{p,q\notin Q_p}\overline{I_pI_q}\approx\frac{1}{N}\sum_{q\in Q_1}\overline{I_1I_q}+\frac{N(N-M)}{N^2}\bar{I}. \tag{A7}$$

By substituting Eq. (A7) in Eq. (A2) one finds that σ_I^2 still scales as N^{-1}, although with a different prefactor:

$$\sigma_I^2=\frac{1}{N}\overline{I_1^2}+\frac{1}{N}\sum_{q\in Q_1}\overline{I_1I_q}-\frac{M}{N}\bar{I}^2. \tag{A8}$$

APPENDIX B: PDF OF c_I

We show here that in the limit of large N and for homogeneous dynamics the PDF of c_I is Gaussian, as found experimentally (see Fig. 5). Additionally, we will demonstrate the relationship $\overline{G_2}=\bar{I}^2(\overline{c_I}+1)$. Note that this relationship is not trivial, since in general $(\overline{c_I}+1)=\overline{[\langle I_pJ_p\rangle_p/IJ]}$ differs from $\overline{\langle I_pJ_p\rangle_p}/\bar{I}\,\bar{J}=\overline{G_2}/\bar{I}^2$.

We start by noting that G_2, I, and J are obtained from an average over a large number N of pixels. Because of the central limit theorem, their PDF is Gaussian, with a standard deviation much smaller than the mean. Accordingly, at any time $G_2(t)=\overline{G_2}[1+\epsilon_{G_2}(t)]$, with ϵ_{G_2} a Gaussian distributed random variable with mean $\overline{\epsilon_{G_2}}=0$ and variance $\sim N^{-1}$. One can write similar expressions for $I(t)$ and $J(t)$, so that to leading order

$$\frac{G_2}{IJ}=\frac{\overline{G_2}(1+\epsilon_{G_2})}{\bar{I}(1+\epsilon_I)\bar{J}(1+\epsilon_J)}\approx\frac{\overline{G_2}}{\bar{I}^2}(1+\xi), \tag{B1}$$

where we have used $\bar{J}=\bar{I}$ and have introduced $\xi=\epsilon_{G_2}-\epsilon_I-\epsilon_J$. ξ is the sum of three (partially correlated) Gaussian random variables and therefore is itself Gaussian distributed [50], with mean $\overline{\epsilon_{G_2}}-\overline{\epsilon_I}-\overline{\epsilon_J}=0$. It follows that the PDF of

$$c_I=\frac{G_2}{IJ}-1\approx\frac{\overline{G_2}}{\bar{I}^2}(1+\xi)-1 \tag{B2}$$

is Gaussian, with mean $\overline{c_I}=\overline{G_2}/\bar{I}^2-1$. Thus, $\overline{G_2}=\bar{I}^2(\overline{c_I}+1)$.

[1] L. Cipelletti and L. Ramos, J. Phys.: Condens. Matter **17**, R253 (2005).
[2] K. Dawson, G. Foffi, M. Fuchs, W. Gotze, F. Sciortino, M. Sperl, P. Tartaglia, T. Voigtmann, and E. Zaccarelli, Phys. Rev. E **63**, 011401 (2001).
[3] T. Eckert and E. Bartsch, Phys. Rev. Lett. **89**, 125701 (2002).
[4] K. N. Pham, A. M. Puertas, J. Bergenholtz, S. U. Egelhaaf, A. Moussaid, P. N. Pusey, A. B. Schofield, M. E. Cates, M. Fuchs, and W. C. K. Poon, Science **296**, 104 (2002).
[5] A. Liu and S. Nagel, Nature (London) **396**, 21 (1998).
[6] L. Cipelletti, S. Manley, R. C. Ball, and D. A. Weitz, Phys. Rev. Lett. **84**, 2275 (2000).
[7] A. Knaebel, M. Bellor, J. P. Munch, V. Viasnoff, F. Lequeux, and J. L. Harden, Europhys. Lett. **52**, 73 (2000).
[8] V. Viasnoff and F. Lequeux, Phys. Rev. Lett. **89**, 065701 (2002).
[9] D. Bonn, S. Tanase, B. Abou, H. Tanaka, and J. Meunier, Phys. Rev. Lett. **89**, 015701 (2002).
[10] E. Weeks, J. Crocker, A. Levitt, A. Schofield, and D. Weitz, Science **287**, 627 (2000).
[11] W. K. Kegel and A. van Blaaderen, Science **287**, 290 (2000).
[12] P. Mayer, H. Bissig, L. Berthier, L. Cipelletti, J. P. Garrahan, P. Sollich, and V. Trappe, Phys. Rev. Lett. **93**, 115701 (2004).
[13] B. J. Berne and R. Pecora, *Dynamic Light Scattering* (Wiley, New York, 1976).
[14] J. W. Goodman, in *Laser Speckles and Related Phenomena, Vol. 9 of Topics in Applied Physics*, edited by J. C. Dainty (Springer-Verlag, Berlin, 1975), p. 9.
[15] D. A. Weitz and D. J. Pine, in *Dynamic Light Scattering*, edited by W. Brown (Clarendon Press, Oxford, 1993), p. 652.
[16] J. Muller and T. Palberg, Prog. Colloid Polym. Sci. **100**, 121 (1996).
[17] K. N. Pham, S. U. Egelhaaf, A. Moussaid, and P. N. Pusey, Rev. Sci. Instrum. **75**, 2419 (2004).
[18] In both methods, different speckles correspond to a different angular orientation of the sample. A given speckle is sampled only once at each sample revolution; thus, the minimum accessible lag is the period of revolution and any spurious decay of the correlation function due to sample rotation is avoided.
[19] A. P. Y. Wong and P. Wiltzius, Rev. Sci. Instrum. **64**, 2547 (1993).
[20] S. Kirsch, V. Frenz, W. Schartl, E. Bartsch, and H. Sillescu, J. Chem. Phys. **104**, 1758 (1996).
[21] L. Cipelletti and D. A. Weitz, Rev. Sci. Instrum. **70**, 3214 (1999).
[22] L. Cipelletti, H. Bissig, V. Trappe, P. Ballesta, and S. Mazoyer, J. Phys.: Condens. Matter **15**, S257 (2003).
[23] V. Viasnoff, F. Lequeux, and D. J. Pine, Rev. Sci. Instrum. **73**, 2336 (2002).
[24] F. Cardinaux, L. Cipelletti, F. Scheffold, and P. Schurtenberger, Europhys. Lett. **57**, 738 (2002).
[25] O. Diat, T. Narayanan, D. L. Abernathy, and G. Grubel, Curr. Opin. Colloid Interface Sci. **3**, 305 (1998).
[26] M. L. Cowan, I. P. Jones, J. H. Page, and D. A. Weitz, Phys. Rev. E **65**, 066605 (2002).
[27] N. Lačević, F. W. Starr, T. B. Schroder, and S. C. Glotzer, J. Chem. Phys. **119**, 7372 (2003).
[28] S. Whitelam, L. Berthier, and J. P. Garrahan, Phys. Rev. E **71**, 026128 (2005).
[29] E. Pitard, Phys. Rev. E **71**, 041504 (2005).
[30] A. de Candia, E. Del Gado, A. Fierro, N. Sator, and A. Coniglio, Physica A **358**, 239 (2005).
[31] N. Lačević, F. W. Starr, T. B. Schroder, V. N. Novikov, and S. C. Glotzer, Phys. Rev. E **66**, 030101 (2002).

[32] H. Bissig, S. Romer, L. Cipelletti, V. Trappe, and P. Schurtenberger, PhysChemComm **6**, 21 (2003).
[33] R. Sarcia and P. Hebraud, Phys. Rev. E **72**, 011402 (2005).
[34] P. Ballesta, C. Ligoure, and L. Cipelletti, AIP Conf. Proc. **708**, 68 (2004).
[35] A. Duri, P. Ballesta, L. Cipelletti, H. Bissig, and V. Trappe, Fluct. Noise Lett. **5**, L1 (2005).
[36] H. Bissig, PhD thesis, University of Fribourg, Fribourg, 2004, also available at http://www.unifr.ch/physics/mm/index.php.
[37] G. Caballero, A. A. Lindner, G. Ovarlez, G. Reydellet, J. Lanuza, and E. Clement, cond-mat/0403604.
[38] C. Chamon, P. Charbonneau, L. F. Cugliandolo, D. R. Reichman, and M. Sellitto, J. Chem. Phys. **121**, 10120 (2004).
[39] M. Clusel, J.-Y. Fortin, and P. C. W. Holdsworth, Phys. Rev. E **70**, 046112 (2004).
[40] M. Merolle, J. P. Garrahan, and D. Chandler, Proc. Natl. Acad. Sci. U.S.A. **102**, 10837 (2005).
[41] A. Crisanti and F. Ritort, Europhys. Lett. **66**, 253 (2004).
[42] S. T. Bramwell, K. Christensen, J.-Y. Fortin, P. C. W. Holdsworth, H. J. Jensen, S. Lise, J. M. Lopez, M. Nicodemi, J.-F. Pinton, and M. Sellitto, Phys. Rev. Lett. **84**, 3744 (2000).
[43] P. A. Lemieux and D. J. Durian, J. Opt. Soc. Am. A **16**, 1651 (1999).
[44] P. A. Lemieux and D. J. Durian, Appl. Opt. **40**, 3984 (2001).
[45] K. Schmidt-Rohr and H. W. Spiess, Phys. Rev. Lett. **66**, 3020 (1991).
[46] M. B. Weissman, Rev. Mod. Phys. **65**, 829 (1993).
[47] D. J. Durian, D. J. Pine, and D. A. Weitz, Science **252**, 686 (1991).
[48] For a foam, $\overline{g_2}$ measured in the transmission geometry is usually fitted by a more complicated expression, which can be found in Ref. [47]. Within the experimental uncertainty, the function of Ref. [47] can be very well approximated by a slightly stretched exponential, which we adopt for the sake of simplicity.
[49] In the linear fit of $\sigma^2_{c_I}$ vs N^{-1}, we weight the data by the inverse of their uncertainty, which we take to be equal to σ_{c_I}.
[50] B. R. Frieden, *Probability, Statistical Optics, and Data Testing* 3rd ed. (Springer, Berlin, 2001).
[51] W. H. Press, B. P. Flannery, S. A. Teukolsky, and W. T. Vetterling, *Numerical Recipes in C++: The Art of Scientific Computing*, 2nd ed. (Cambridge University Press, Cambridge, 2002).
[52] O. Glatter, J. Appl. Crystallogr. **10**, 415 (1977).
[53] O. Glatter, in *Neutrons, X-rays and Light: Scattering Methods Applied to Soft Condensed Matter*, edited by P. Lindner and T. Zemb (North-Holland, Amsterdam, 2002)
[54] The so-called speckle visibility spectroscopy method introduced in Refs. [64,65] and discussed briefly in the conclusions addresses the case where $c_I(t,0)$ fluctuates on the time scale of the CCD exposure time, because of dynamical heterogeneity.
[55] To evaluate σ^2_ϵ, we take a time series of dark images. To each dark image we then add, pixel-by-pixel, the intensity distribution of one single image of the speckle pattern scattered by the sample. In the series thus obtained, all images are identical, except for the small fluctuations due to $\epsilon_p(t)$. This corresponds to what would be obtained for a perfectly frozen scatter, in the absence of all possible experimental artifacts, as discussed in Sec. VI. We process the data as usual and calculate the variance of c_I. For all lags $\tau > 0$ the same value is obtained, which is taken as an estimate of σ^2_ϵ.
[56] F. Castro-Roman, G. Porte, and C. Ligoure, Phys. Rev. Lett. **82**, 109 (1999).
[57] P. T. Tokumaru and P. E. Dimotakis, Exp. Fluids **19**, 1 (1995).
[58] We neglect refractions at the solvent-container and container-air interfaces, since they only displace the beam parallel to itself.
[59] G. Parry, Opt. Commun. **12**, 75 (1974).
[60] T. M. Lehmann, C. Gonner, and K. Spitzer, IEEE Trans. Med. Imaging **18**, 1049 (1999).
[61] H. Bissig, V. Trappe, S. Romer, and L. Cipelletti, cond-mat/0301265.
[62] P. Ballesta, A. Duri, and L. Cipelletti (in preparation).
[63] D. El Masri, M. Pierno, L. Berthier, and L. Cipelletti, J. Phys.: Condens. Matter **17**, 53543 (2005).
[64] P. K. Dixon and D. J. Durian, Phys. Rev. Lett. **90**, 184302 (2003).
[65] R. Bandyopadhyay, A. Gittings, S. Suh, P. Dixon, and D. J. Durian, Rev. Sci. Instrum. **76**, 093110 (2005).
[66] P. Habdas and E. R. Weeks, Curr. Opin. Colloid Interface Sci. **7**, 196 (2002).
[67] L. Buisson, L. Bellon, and S. Ciliberto, J. Phys.: Condens. Matter **15**, S1163 (2003).
[68] L. Bellon, L. Buisson, S. Ciliberto, and F. Vittoz, Rev. Sci. Instrum. **73**, 3286 (2002).